

Importin-binding Regulates Contractile Proteins

for Cytokinesis

Nhat Phi Pham

A Thesis

In the Department

of

Biology

Presented in Partial Fulfilment of the Requirements

For the Degree of

Master of Science (Biology) at

Concordia University

Montreal, Quebec, Canada

August 2020

© Nhat Phi Pham, 2020

CONCORDIA UNIVERSITY
School of Graduate Studies

This is to certify that the thesis prepared

By: Nhat Phi Pham

Entitled: Importin-binding Regulates Contractile Proteins for Cytokinesis

and submitted in partial fulfilment of the requirements for the degree of

Master of Science (Biology)

complies with the regulations of the University and meets the accepted standards with respect to its originality and quality.

Signed by the final Examining Committee:

_____ Chair

Dr. Michael Sacher

_____ External Examiner

Dr. Peter Darlington

_____ Examiner

Dr. Peter Pawelek

_____ Examiner

Dr. Michael Sacher

_____ Supervisor

Dr. Alisa Piekny

Approved by

Dr. Robert Weladji, Graduate Program Director

_____ 2020

Pascale Sicotte, Dean of Faculty

Abstract

Importin-binding regulates contractile proteins for cytokinesis

Nhat Phi Pham

Cytokinesis, the last step of mitosis, describes the physical separation of a cell into two daughters. In metazoan cells, a contractile ring composed of actin and myosin forms at the division plane and constricts the plasma membrane of the cell. Failure to complete cytokinesis or aberrant cell division can result in changes in fate or cause aneuploidy, both of which are hallmarks of cancer and other pathologies. To ensure that the assembly and constriction of the contractile ring is spatiotemporally coordinated with chromosome segregation, multiple pathways function cooperatively to regulate the localization and function of contractile proteins. These include pathways from the mitotic spindle, which provides cues for ring assembly and positioning. In addition, our lab recently uncovered a novel pathway which senses chromatin to position the ring. The work described here helped to elucidate the molecular mechanisms by which spindle-dependent and -independent pathways work together for cytokinesis, and to find novel targets of the chromatin pathway. Here, we show how the binding of importins, microtubules and RhoA are coordinated to regulate the scaffold protein anillin for cytokinesis. We also show that the NLS of Ect2, the activator of RhoA, is required for cytokinesis. Finally, to identify other contractile proteins regulated the Ran pathway in cytokinesis, a BioID of importin- β 1 identified 206 potential new mitotic proximity interactors.

Acknowledgements and Dedications

I thank Dr. Alisa Piekny for giving me the opportunity to study in her lab. Thank you, Alisa, for your patience, trust, and generosity. I am grateful for the time you give us, and all the hard work you put in to guide our projects. Thank you for challenging us to be better scientists.

I thank my committee members, Dr. Michael Sacher and Dr. Peter Pawelek, as well as Dr. Peter John Darlington, for their time and consideration. I thank you for the invaluable insight you have provided to this project.

I am grateful to Dr. Chris Law, the operations manager of the *Centre for Microscopy and Cellular Imaging* (CMCI) at Concordia. Thank you for teaching me how to operate the CMCI's intimidating microscopes and for helping me through technological crises.

Thank you to Heng Jiang, the Applications Specialist of the *Centre for Biological Applications of Mass Spectrometry*. Thank you for your patience and encouragement. Your guidance was an incredible asset for our BioID experiments.

I would like to thank the past and present members of the Piekny lab for all their help, time, and insight. Thank you, Danny, for mentoring me and introducing me to the project. I will remember our RhoA pull-downs fondly. Noha, working with you has been a joy – thank you for your unwavering positive attitude. Su Pin, if it were not for you, the BioID project would not be where it is today. Thank you for your brilliance and for keeping us organized. Ìmge, thank you for sharing your knowledge of Ran, importins and anillin with me, as well as for your magical friendship. Kevin, you are our rock in tissue culture, and I am deeply grateful for your expertise. I treasure our conversations and the perspective you offer. Mathieu, your indefatigable zeal in the lab has been an inspiration. Thank you for your help with plasmid design, and for forging the mNeonGreen-Ect2 cell line. Joe, thank you for your continued help in elucidating the mystery of

Ect2 regulation. Victoria, you are a wonderful addition to the lab, and I am thankful to work in your company. I would also like to thank Dr. Steph, Dilan, and Karina for helpful conversations. Last but not least, special thanks go to Mathew for performing the maintenance work that supports our research.

I dedicate this thesis to my mother. Thank you, mom, for raising me and for supporting my studies. You have made all of this possible. Love you.

Contribution of Authors

Figure 6. This figure was made in collaboration with Daniel Beaudet. Daniel Beaudet and I both contributed to the Coomassie-stained gels and quantifications.

Figure 7. The FRAP experiments were performed by Daniel Beaudet.

Figure 8. This figure was made in collaboration with Daniel Beaudet. Daniel Beaudet and I both contributed to the immunoblots. Daniel Beaudet drew the models and performed live-imaging.

Figure 9. The model was drawn by Daniel Beaudet.

Figure 11. This figure was made in collaboration with Joseph Del Corpo.

Figure 13. This figure was made in collaboration with Su Pin Koh.

Table 1. This table was made in collaboration with Su Pin Koh.

Table of Contents

List of Figures and Tables	ix
List of Abbreviations	x
Chapter 1: Introduction	1
1.1 Cytokinesis and cell division	1
1.2 Cytokinesis regulators	2
1.3 Spindle-dependent pathways.....	5
1.4 Spindle-independent pathways.....	9
1.5 The chromatin-sensing pathway	12
1.6 Thesis summary	14
Chapter 2: Materials & Methods	18
2.1 Cell culture	18
2.2 Plasmids.....	18
2.3 Microscopy and immunostaining.....	19
2.4 Rescue assay	22
2.5 Protein purification and pull-downs	22
2.6 Co-sedimentation assays	23
2.7 Proximity-based biotinylation and mass spectrometry analysis.....	24
2.8 Analysis of mass spectrometry data	26
Chapter 3: Results	27

3.1. The cortical properties of anillin are regulated differently by importins and microtubules	27
3.2. RhoA and importins feedback to recruit anillin to the cortex.....	34
3.3. Ect2 as a potential target of the Ran pathway during cytokinesis.....	39
3.4 Identifying new targets of the Ran pathway during cytokinesis	44
Chapter 4: Discussion	50
Chapter 5: References	59

List of Figures and Tables

Figure 1. Schematic of a cell undergoing mitosis.....	3
Figure 2. Multiple pathways regulate cytokinesis.....	8
Figure 3. Structure of Anillin and Ect2.	10
Figure 4. Ran-GTP and importins regulate the recruitment of anillin to the cleavage furrow.....	15
Figure 5. The NLS of anillin is required for importin-binding in vitro.....	28
Figure 6. Importin and microtubules partially compete for anillin-binding.....	29
Figure 7. Importins and microtubules regulate distinct cortical properties of anillin.	33
Figure 8. Anillin requires RhoA-binding, importin-binding and the interface between the RBD and C2 for its localization and function in cytokinesis.....	36
Figure 9. A model for how importin-binding facilitates the RhoA-mediated recruitment of anillin to the membrane during cytokinesis.....	38
Figure 10. A conformational change in Ect2 is required for its activity.....	40
Figure 11. The NLS of Ect2 is required for its function during cytokinesis.	41
Figure 12. Time-lapse microscopy of Ect2-mNeonGreen in a dividing HeLa cell.....	43
Figure 13. Identification of the importin- β 1 proximity interactome in mitosis using BioID.	47
Table 1. Importin- β 1 interactors common to BIOGRID are enriched in the experimental BioID dataset.....	49

List of Abbreviations

AHD	Anillin Homology domain
BIOGRID	Biological General Repository for Interaction Datasets
BioID	Proximity-based biotinylation assay
BKGD	Background
BRCT	BRCA1 C-terminal
C2	Protein kinase C conserved lipid binding region 2
Cdc42	Cell division control protein 42
Cdk1	Cyclin-dependent kinase 1
cDNA	Complementary DNA
C-term	C-terminus or carboxyl-terminus
Cyk4	Cytokinesis defect 4 [or MgcRacGAP (Male germ cell RacGAP (RacGTPase activating protein)) rho-family GAP in humans; RacGAP50C in <i>Drosophila</i>]
DAPI	4',6-diamidino-2'-phenylindole dihydrochloride
DAVID	Database for Annotation, Visualization and Integrated Discovery
DH	Dbl (diffuse B-cell lymphoma) homology
DNA	Deoxyribunucleic acids
Ect2	Epithelial cell transforming 2
FL	Full length
FRAP	Fluorescence recovery after photobleaching
FRET	Förster resonance energy transfer
GAP	GTPase activating protein
GDP	Guanosine diphosphate
GEF	Guanosine nucleotide exchange factor
GFP	Green fluorescent protein
GST	Glutathione S-transferase
GTP	Guanosine triphosphate

GTPase	Guanosine triphosphatase
HEK293	Human embryonic kidney 293
HeLa	Henrietta Lacks (uterine cells derived from)
His	Poly-histidine tag
I/F	Interface
Imp- β	Importin- β nuclear transport receptors
KPNB1	Karyopherin- β 1 or importin- β 1
LUTs	Look up tables
M.W.	Molecular weight
MBP	Maltose binding protein
MCAK	Mitotic centromere-associated kinase
mCherry	Monomeric cherry fluorescent protein
MKLP1	Mitotic kinesin like protein 1
mNeonGreen	monomeric Neon Green
MT	Microtubules
Myc	Polypeptide affinity protein tag derived from cMyc
n.s.	Not significant
NLS	Nuclear Localization Sequence
N-term	N-terminus or NH ₂ -terminus
P	pellet
<i>Pebble</i>	<i>Drosophila</i> homolog of Ect2
PH	Pleckstrin homology
PI(4,5)P ₂	Phosphatidylinositol 4,5-bisphosphate
Plk1	Polo-like kinase 1
PP1-Sds22	Protein phosphatase 1 and its regulatory subunit Sds22
Ptk1	<i>Potorous tridactylus</i> kidney 1
Rac	Ras-related C3 botulinum toxin substrate protein RacGAP50C in <i>Drosophila</i>]
Ran	Ras-related nuclear protein GTPase
RanGAP	Ran GTPase activating protein

RBD	Rho-binding domain
RCC1	Regulator of chromosome condensation 1
RhoA	Ras homolog family member A
RNAi	Ribonucleic Acid interference
ROCK	Rho-associated protein kinase
ROI	Region of interest
S	Supernatant
SAF	Spindle assembly factor
SD	Standard deviation
SEM	Standard error of the mean
siRNA	Small interfering ribonucleic acid

Chapter 1: Introduction

1.1 Cytokinesis and cell division

The cell cycle of eukaryotes is divided into the G1, S, G2 and M phases (McIntosh 2016). Interphase spans the G1, S and G2 phases, and describes the stages during which biosynthesis of proteins and the replication of genomic DNA occur. The cell cycle is regulated by the activity of cyclins and cyclin-dependent kinases (Cdks); the binding of a cyclin and Cdk determines the kinase's activity and specificity, and phosphorylation of proteins by Cdks can activate or inactivate a protein for a specific stage of the cell cycle. In M-phase, or mitosis, the cell undergoes extensive rearrangement of its cytoskeleton, the nuclear envelope breaks down, the chromosomes align at the cell equator and are segregated. Cytokinesis, the last step of mitosis, describes the formation of a contractile ring between the segregating chromosomes, which pinches the membrane to physically separate the dividing cell into two daughter cells.

Multiple pathways ensure that the assembly and constriction of the contractile ring is spatiotemporally coupled with the segregation of DNA and cell fate determinants. While cytokinesis is described as the last step of mitosis, the formation of the contractile ring begins in anaphase, as the chromosomes are segregated to opposite poles. Signals from the central spindle – an array of antiparallel microtubules which forms between the segregating chromosomes – positively regulate the GTPase RhoA for the assembly of the contractile ring. In addition, emanating from the poles of the cell are astral microtubules, which negatively regulate proteins at the poles to ensure the narrow recruitment of contractile proteins to the equatorial cortex. Signals independent of microtubules, such as proteins localized at the cortex, kinetochores or near DNA can also influence the localization of cytokinesis proteins at the cleavage furrow. Although the requirements for these pathways are unclear and differ between different cell types and organisms, these pathways cooperate to tightly regulate cytokinesis.

1.2 Cytokinesis regulators

In anaphase, several key regulators of cytokinesis are recruited to the equatorial cortex to assemble the contractile ring. The process of ring assembly begins with the activation of the GTPase RhoA – known as the master regulator of cytokinesis – by the GEF Ect2 at the cell equator. In its active, GTP-bound form, RhoA recruits and activates profilins and formins, which nucleate linear actin filaments, and the kinase ROCK, which promotes the assembly of non muscle myosin II filaments (Matsumura et al. 1998; Kosako et al. 2000; Alberts 2001). The phosphorylation of the regulatory light chain (RLC) by ROCK promotes the assembly of bipolar myosin filaments and allows myosin to interact with actin. Myosin light chain phosphatase (MLCP) dephosphorylates the RLC, however ROCK also can phosphorylate and inactivate MLCP (Kimura et al. 1996). Thus, the balance of ROCK and MLCP activities is crucial for contractile ring formation (Piekny and Mains, 2002). This RhoA-dependent signaling cascade leads to the formation of an actomyosin ring, and the procession of the motor protein myosin along actin filaments generates the force required for constricting the dividing cell into two daughters.

RhoA activation is regulated by Ect2 in a cell-cycle dependent manner. The GEF Ect2 is essential for cytokinesis, and its depletion or inhibition causes cytokinesis failure and multinucleation. Ect2 consists of N-terminal BRCT repeats, an 'S-loop' with an NLS(s), and C-terminal DH- and PH- domains. The catalytic DH domain binds to RhoA and mediates GEF activity, whereas the PH domain binds to lipids. Both domains are crucial for Ect2 function and the activation of RhoA (Frenette et al. 2012). In early mitosis, the phosphorylation of Ect2 by the kinase Cdk1 at Thr342 has been proposed to cause auto-inhibition of the C-terminus by the BRCT domains. This auto-inhibition is presumably relieved during anaphase when Cdk1 activity drops and this site is dephosphorylated and by binding to Cyk4 (Tatsumoto et al. 1999; Saito et al. 2004; Yüce et al. 2005; Hara et al. 2006). Ect2 is recruited to the central spindle via its association to Cyk4, and, through an unclear mechanism, is recruited to the equatorial membrane where it

activates RhoA to initiate ring assembly.

The scaffold protein anillin is a crucial regulator of cytokinesis that is also recruited to the cleavage furrow by RhoA. Anillin tethers the actomyosin contractile ring to the cell membrane. In anillin-depleted human or *Drosophila* S2 cells, the contractile ring oscillates followed by furrow regression and the cells become binucleate (Straight et al. 2005; Zhao and Fang 2005; Hickson and O'Farrell 2008; Piekny and Glotzer 2008). Anillin binds directly to the contractile ring via its N-terminal actin and myosin binding domains (Field and Alberts 1995; Straight et al. 2005). An N-terminal NLS mediates anillin's nuclear localization (Oegema et al. 2000; Chen et al. 2015). The C-terminal half of anillin has a RhoA binding domain (RBD), a C2 domain with binding sites for microtubules, phospholipids, importins and Ect2, and a PH domain that also binds to phospholipids and septins (Piekny and Glotzer 2008; Tse et al. 2011; Frenette et al. 2012; van Oostende Triplet et al. 2014; Chen et al. 2015; Sun et al. 2015; Beaudet et al. 2017).

In addition to positioning the ring via crosslinking actomyosin with the membrane, anillin appears to feedback to stabilize RhoA and promote its own recruitment to the furrow (Piekny and Glotzer 2008; Budnar et al., 2019). For example, it could promote RhoA activity via a 'resetting' mechanism involving the accumulation of PI(4,5)P2 at the cleavage furrow via its L3 loop (Budnar et al. 2019). The phospholipid PI(4,5)P2 is required for RhoA's association with the membrane. In this model, anillin concentrates PI(4,5)P2 at the membrane, which increases RhoA membrane retention and thus promotes RhoA signaling to effector proteins at the cleavage site. Upon RhoA dissociating from the membrane, the presence of anillin and PI(4,5)P2 at the membrane would favour RhoA's re-association with the membrane, hence the 'resetting' mechanism. Since binding to RhoA increases anillin's avidity for the cortex, stabilizing RhoA feedbacks to stabilize anillin at the membrane (Sun et al. 2015).

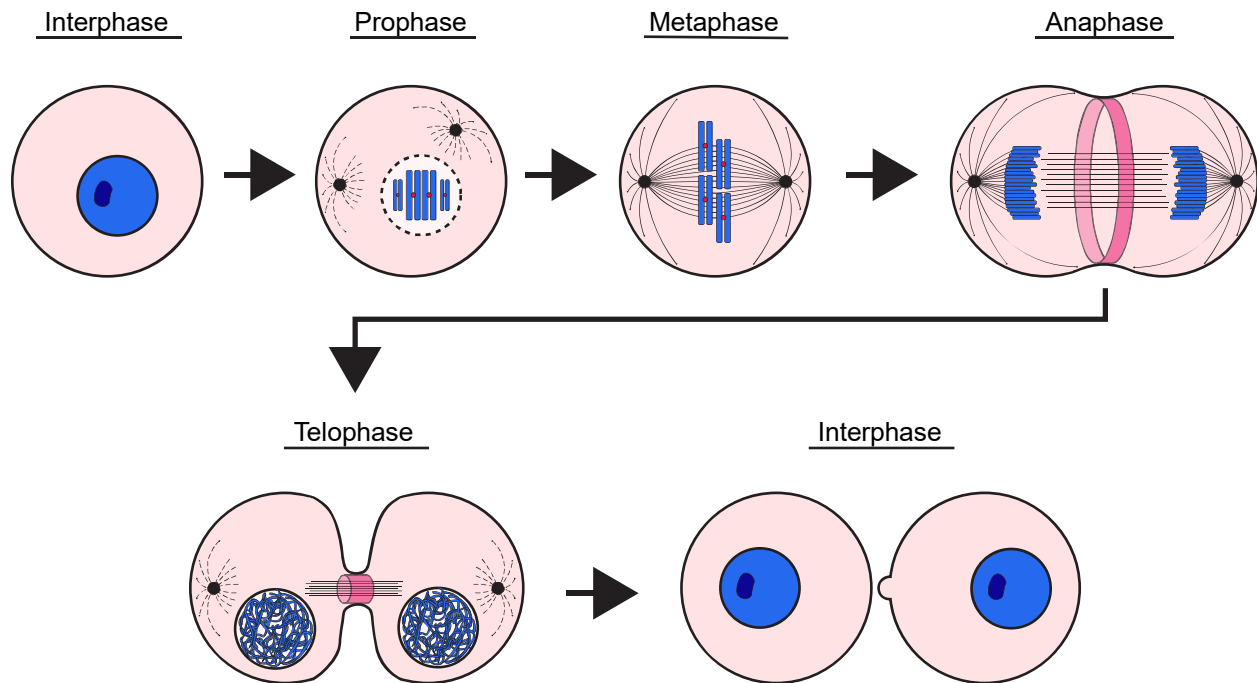


Figure 1. Schematic of a cell undergoing mitosis. Interphase cells replicate genomic material in preparation for mitosis. In prophase, nuclear envelope breakdown (NEBD) occurs and centrosomes mature and begin to separate. In metaphase, a bipolar spindle has formed with sister chromatids aligned at the cell equator. In anaphase, the central spindle arises between sister chromatids as they segregate to opposite poles. The contractile ring begins to assemble. In telophase, the ring matures and ingresses, the chromatin begins to decondense and the nuclear envelope reforms. The central spindle and contractile ring subsequently forms a midbody that mediates abscission. The two daughter cells then enter G1. Thus, cytokinesis spans anaphase and telophase, and includes contractile ring assembly, constriction, formation of the midbody and abscission.

1.3 Spindle-dependent pathways

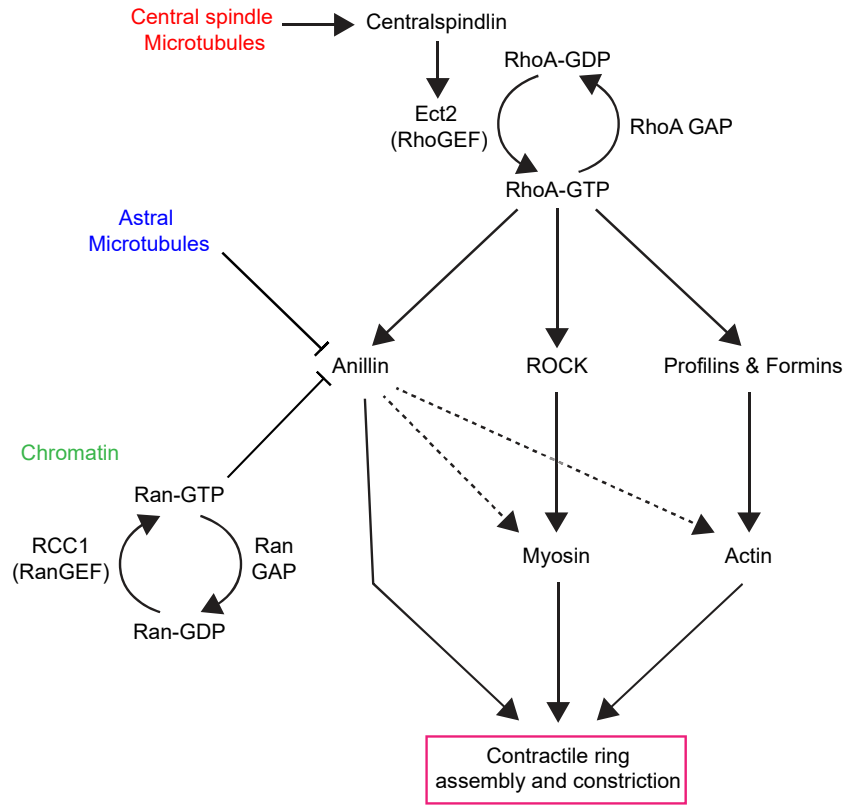
The mitotic spindle provides both stimulatory and inhibitory cues to regulate cytokinesis. The anaphase spindle is composed of astral microtubules that extend radially from the centrosomes to the poles of the dividing cell, and the central spindle, which is composed of anti-parallel microtubules that arise between segregating chromosomes and are cross-linked by various complexes (Glotzer 2005). The central spindle is considered 'stimulatory' because the centralspindlin complex, a heterotetramer of MgcRacGAP and MKLP1 (Mishima et al. 2002), recruits and activates the GEF Ect2 at the overlying cortex (Yüce et al. 2005; Kamijo et al. 2006). Ect2 forms a cell-cycle-dependent complex with MgcRacGAP at the cell equator where it generates active RhoA. In its active GTP-bound conformation, RhoA-GTP initiates the recruitment and activation of effector proteins which assemble and constrict the contractile ring as described in 1.1 (Bement et al. 2005). In *Drosophila* embryos, *Pebble* (Ect2 homolog) or RacGAP50C (MgcRacGAP homologue) mutants fail cytokinesis, and their interaction is required for cytokinesis (Somers and Saint 2003; Piekny et al. 2005). The same relationship was observed in echinoderm embryos and mammalian cells: depletion of MgcRacGAP or Ect2, or mutations that disrupt their interaction caused cytokinesis failure due to decreased RhoA activation and failure to form a contractile ring (Bement et al., 2005; Yüce et al. 2005).

There are two ways in which the centralspindlin complex could be regulated for cytokinesis. First, the MgcRacGAP-Ect2 complex must form at the membrane for its function, and central spindle localization is dispensable (Su et al. 2011; Lekomtsev et al. 2012; Kotýnková et al. 2016). However, Cyk4 requires phosphorylation by Plk1 prior to binding Ect2 (Petronczki et al. 2007; Burkard et al. 2009; Wolfe et al. 2009; Kim et al. 2014; Zou et al. 2014), and since Plk1 is localized to the central spindle and activated by PRC1 (Wolfe et al. 2009), the spindle has been proposed to function as a 'sink' for the Cyk4-MKLP1 complex (Adriaans et al. 2019). Centralspindlin localizes to the central spindle where the MKLP1 subunit bundles microtubules,

and Cyk4 can be phosphorylated by Plk1. This phosphorylation could release the complex to the cortex to associate with Ect2. Second, the Cyk-4-MKLP1 complex can also be regulated by Aurora B kinase. MKLP1 can be bound by 14-3-3, which sequesters it and prevents clustering of the centralspindlin complex that is required for central spindle formation (Douglas et al. 2010; Basant et al. 2015). When MKLP1 is phosphorylated by Aurora B kinase, this hinders 14-3-3 binding, releasing it. Active Aurora B kinase localizes to the kinetochores and central spindle, where it could release complexes at or near the equatorial cortex. It is not well-understood how this could affect Ect2 activity, but Aurora B activity presumably also increases accessibility to Cyk-4 for Ect2-binding. It is also not clear how these complexes generate a tight zone of active Ect2 and RhoA at the equatorial membrane for contractile ring assembly.

Astral microtubules negatively regulate contractility during cytokinesis, although the mechanisms by which they do this are not clear. Studies in human cells and *C. elegans* showed that perturbing astral microtubule dynamics leads to changes in the localization of contractile proteins and furrowing phenotypes. In *C. elegans* embryos, a higher density of astral microtubules at the cortex inhibits furrow ingression (Dechant and Glotzer 2003). In the same model, laser-ablation of one of the two asters caused an additional furrow to form and the position of this additional furrow was dependent on which aster was ablated (Bringmann and Hyman 2005). This aster-dependent furrow formed before the midzone-directed furrow. Similarly, preventing the separation of asters during anaphase caused ectopic furrowing and delayed furrow formation (Lewellyn et al. 2010). Taken together, these data suggest that the astral microtubules act to restrict the localization of contractile proteins before the central spindle signals to the cortex, and thereafter continues to support a robust and narrow cleavage furrow. In gamma-tubulin depleted *C. elegans* embryos, contact between dynamic microtubules of a monopolar spindle and the cortex cleared myosin from the cortex (Werner et al. 2007). Subsequent studies showed that anillin also binds to microtubules in human cells and *C. elegans*, which could remove it from the

A



B

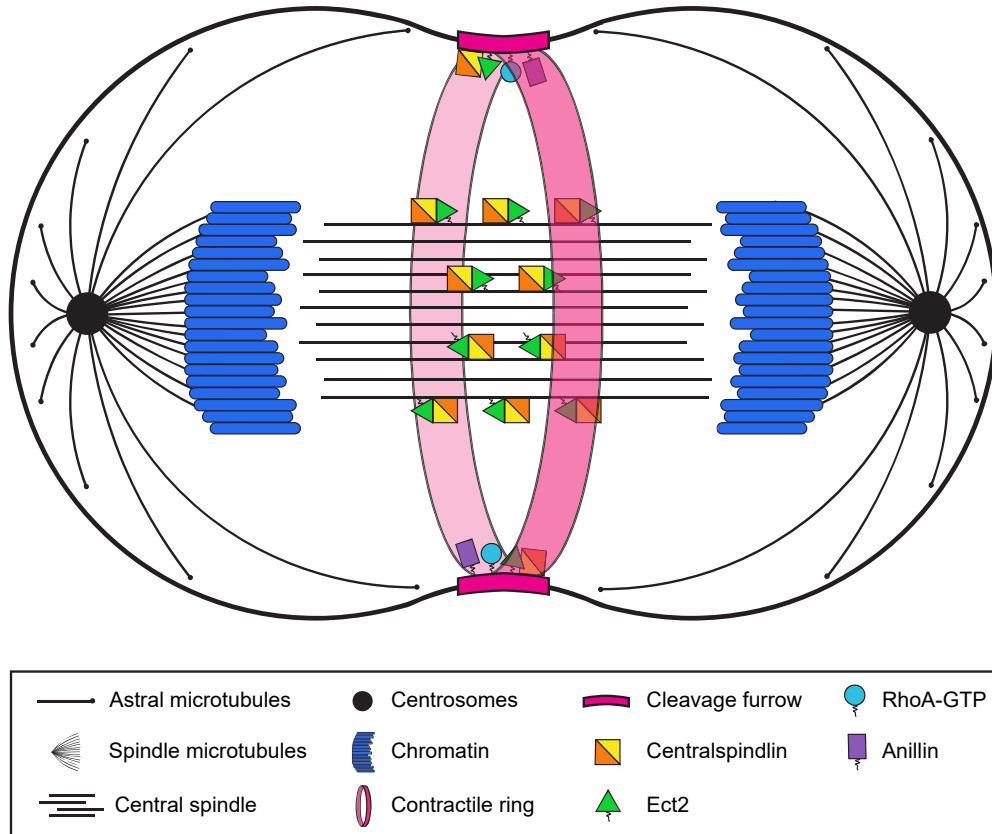


Figure 2. Multiple pathways regulate cytokinesis. (A) Some of the different pathways that regulate cytokinesis are shown. Astral microtubules negatively regulate the localization of contractile proteins at the polar cortex, ensuring the discrete localization of these proteins at the equatorial plane. The central spindle microtubules recruit centralspindlin and Ect2, which activates RhoA at the overlying membrane. Active RhoA recruits effector proteins to assemble the contractile ring. Anillin, a scaffold protein, crosslinks the actomyosin ring to the membrane to control its position. A chromatin-associated pathway (Ran-GTP) regulates the localization of anillin through importin-binding. (B) A cartoon schematic shows a cell in late anaphase/early telophase as the contractile ring matures. The relative localization of key cytokinesis regulators (RhoA, anillin, Ect2 and centralspindlin) is shown.

polar cortex (Tse et al. 2011; van Oostende Triplet et al. 2014). The depletion of astral microtubules in cultured human cells using a low concentration of nocodazole, which depolymerizes microtubules, caused an increase in the breadth of RhoA and myosin, which extended into the polar cortex (Murthy and Wadsworth 2008; van Oostende Triplet et al. 2014). Similarly, depleting astral microtubules in fixed echinoderm cells caused the global localization of active myosin (Foe and Von Dassow 2008). Contrastingly, extending astral microtubules by depleting MCAK, an enzyme that depolymerizes microtubules, in cultured human cells narrowed the breadth of myosin, anillin and RhoA at the cell equator (Zanin et al. 2013; van Oostende Triplet et al. 2014). Myosin localization was restored by depleting anillin, which indicates that astral microtubules regulate myosin localization through anillin (van Oostende Triplet et al. 2014).

While the mechanism through which asters inhibit protein localization at the polar cortex is still unclear, the clearing of anillin from the polar cortex has been shown to be dependent on TPX2 and Aurora A (Mangal et al. 2018). Moreover, points of contact between stable pools of astral microtubules coincide with bright foci of active myosin, suggesting that stable and dynamic microtubules may play opposite roles in cytokinesis (Foe and Von Dassow 2008).

1.4 Spindle-independent pathways

Signals from the cortex, kinetochores and chromatin also regulate cytokinesis. Ptk1 cells treated with nocodazole to disassemble microtubules retained furrowing (Canman et al. 2000). In asymmetrically dividing *Drosophila* neuroblasts, colcemid treatment to ablate microtubules showed that the basally displaced furrow can still form without microtubules (Cabernard et al. 2010). Rotating or displacing the mitotic spindle in these cells revealed that two furrows can form: one mediated by the central spindle and one mediated by the Pins complex (Cabernard et al. 2010). The Pins complex, localized to the apical cortex, polarizes myosin localization to the basal

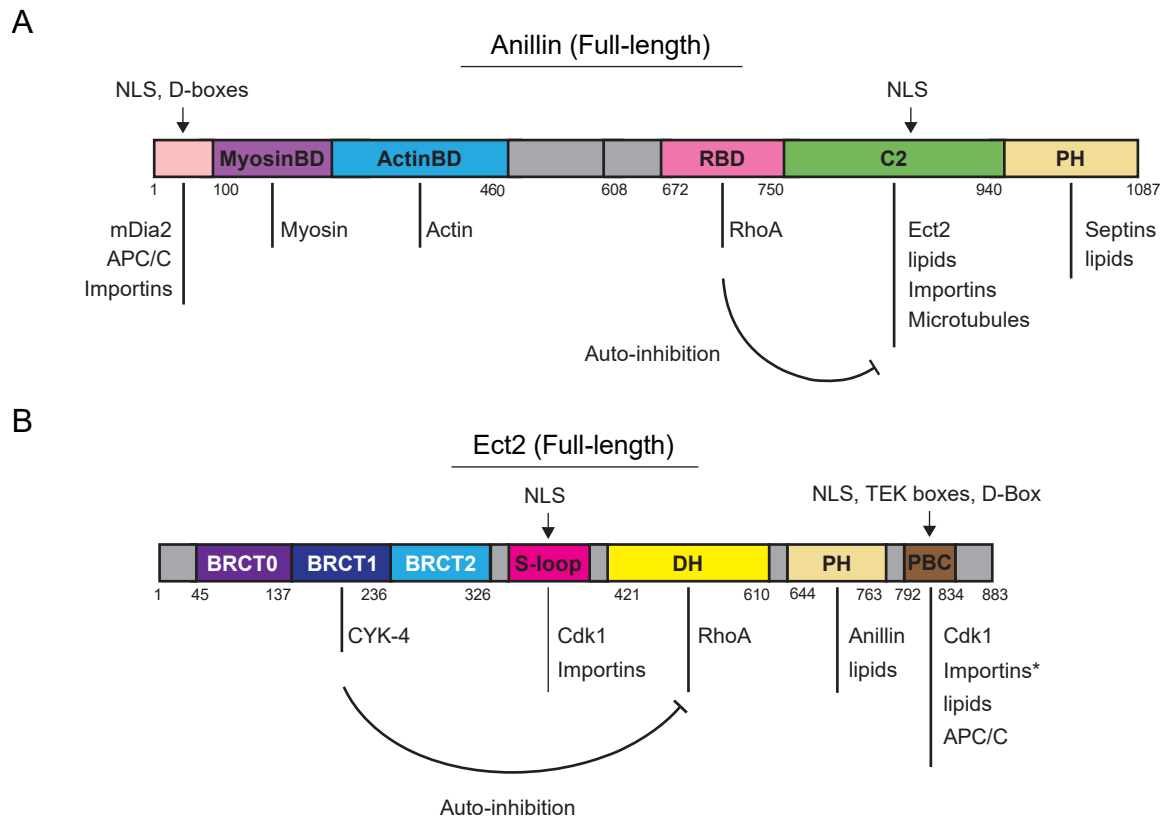


Figure 3. Structure of Anillin and Ect2. (A) A cartoon shows the structure of anillin with the location of the various binding domains. Anillin tethers the contractile ring to the membrane by binding to actin and myosin with its N-terminal domains and to RhoA and lipids with its C-terminal domains. The RBD inhibits the C2 domain. (B) A cartoon shows the structure of Ect2 with location of the various binding domains. The C-terminus of Ect2 is inhibited by the N-terminal BRCTs due to phosphorylation of a Cdk1 site in the S-loop. Dephosphorylation at this site coupled with binding to CYK-4 presumably relieves this auto-inhibition, enabling Ect2 to activate RhoA.

cortex in the absence of a central spindle. Similarly, in mammalian cells, the GTPase activating protein MP-GAP globally inhibits RhoA at the cortex in mitosis; depleting MP-GAP leads to RhoA-dependent hypercontractility throughout the cell cortex (Zanin et al. 2013). This global inhibition of RhoA by MP-GAP is proposed to be relieved at the cell equator due to the persistent GEF activity of Ect2 (Zanin et al. 2013). Furthermore, the novel protein NOP-1 discovered in *C. elegans* was found to promote the accumulation of myosin, anillin and actin at pseudocleavage furrows, which form in the oocyte at the time of sperm entry (Tse et al. 2012). NOP-1 localizes to the cytosol and to the ingressing furrows and is hypothesized to function redundantly with CYK-4 to regulate ECT-2 activity during cytokinesis of the one-cell embryo (Tse et al. 2012).

Kinetochores polarize the cortex through the activity of the PP1-Sds22 phosphatase complex, which dephosphorylates the actin crosslinker moesin (Rodrigues et al. 2015). The proximity of kinetochore-associated PP1-Sds22 to the membrane is associated with local dephosphorylation of moesin and clearing of actin at the polar cortex; inhibiting the recruitment of PP1-Sds22 to kinetochores or preventing the dephosphorylation of moesin by expressing a phosphomimetic mutant abolished cortical polarization (Rodrigues et al. 2015).

Proximity to chromatin also regulates cortical polarization. Several groups observed that the cortex of dividing cells responds to chromatin proximity. For example, elongating chromatid arms in *Drosophila* neuroblasts led to broader myosin localization at the cleavage furrow (Kotadia et al. 2012). Similarly, when chromatin moved close to the polar cortex in cultured mammalian cells, contractile proteins cleared from the nearby cortex (Kiyomitsu and Cheeseman, 2013). This was demonstrated to be dependent on active Ran GTPase, and work from our lab has elucidated the mechanism by which chromatin sensing controls cytokinesis via regulating anillin function and is described in the next section.

1.5 The chromatin-sensing pathway

The GTPase Ran functions to control multiple biological processes, and one of its best-understood roles is to regulate nucleocytoplasmic transport in interphase cells (reviewed in Clarke and Zhang 2008). Briefly, proteins with a nuclear localization sequence (NLS) are recognized by importin-alpha, which binds to this region together with importin-beta. The heterodimer mediates transport of the NLS-protein into the nucleus through nuclear pore complexes. In the nucleus, high levels of active, GTP-bound Ran causes importins to dissociate from the NLS-protein where it presumably remains. The nucleus is enriched with Ran-GTP due to the active shuttling of Ran into the nucleus by NTF2 and the presence of the RanGEF RCC1, which is tethered to chromatin. In contrast, the cytoplasm is enriched with inactive, Ran-GDP due to the cytosolic localization of RanGAPs which promote GTP-hydrolysis. Elegant experiments in sea urchin embryos using FRET probes confirmed the strong enrichment of Ran-GTP in the nucleus vs. the cytoplasm (Kalab et al. 2002).

Due to nuclear envelope breakdown in mitosis, Ran-GTP exists as a gradient in dividing cells. Since RanGAPs are present in the cytoplasm and RCC1 is tethered to chromatin, Ran-GTP concentration is highest near chromatin and lowest at the cortex away from chromatin (Kalab et al. 2002; Kaláb et al. 2006). This gradient was visualized by FRET probes in sea urchin embryos and mammalian cells. In mitosis, Ran promotes the assembly of the mitotic spindle assembly. The binding of Ran-GTP relieves the inhibition of spindle assembly factors (SAFs) by importins in the vicinity of chromatin (Walczak and Heald 2008). Multiple SAFs are known to be regulated in this manner, such as TPX2, XCTK2, Rae1, Maskin and Lamin B (Schatz et al. 2003; Tsai et al. 2003; Ems-McClung et al. 2004; Blower et al. 2005; Albee et al. 2006; Tsai et al. 2006; Weaver et al. 2015).

Ran-GTP was also shown to control cortical polarity. The injection of DNA-coated beads in mouse oocytes caused the formation of local actin caps and myosin rings required for polar

body extrusion during meiosis (Deng et al. 2007). These structures were abolished or decreased by the addition of RanT24N, a dominant negative Ran mutant which inhibits generation of Ran-GTP (Deng et al. 2007). In the same model, the GTPase Cdc42 was found to localize near chromosomes in a Ran-GTP-dependent manner; here again, injecting RanT24N abolished Cdc42 cortical localization (Dehapiot et al. 2013). Cdc42 presumably is required in these cells for polar body formation by activating N-WASP, which recruits the actin nucleator Arp2/3 (Dehapiot et al. 2013). Furthermore, upon RanT24N injection, phosphorylated ezrin/radixin/moesin (ERM) proteins were no longer localized in a polarized manner and were found globally around the cortex (Dehapiot and Halet 2013). A model was proposed where active Ran forms a gradient relative to chromatin position and functions as a molecular ruler to define cortical polarity. The ruler function was proposed because there was an optimal distance from chromatin where the cortex polarized.

Recent studies in mammalian cells showed that Ran-GTP also controls cortical polarity during cytokinesis. Cells elongate in response to chromatin to re-define the equatorial plane and ensure that furrowing occurs at a position that bisects the segregated chromosomes (Kiyomitsu and Cheeseman 2013). In a subset of HeLa cells where the spindle was misplaced, proximity to chromatin was associated with cell elongation and the clearing of anillin and myosin at the side of the cortex where elongation occurred (Kiyomitsu and Cheeseman 2013). Baby hamster kidney epithelial cells (BHK) harboring a temperature-sensitive allele of RCC1 revealed that cortical polarization is Ran-GTP-dependent, as anillin failed to clear from the cortex of cells lacking microtubules and forced to exit mitosis at restrictive temperature (Kiyomitsu and Cheeseman 2013). Our lab subsequently used the same BHK cells to show that Ran-GTP levels control the localization of contractile proteins in cells with intact spindles during cytokinesis (Beaudet et al. 2017). In addition, artificially targeting constitutively active Ran(Q69L) to the cortex disrupted anillin's cortical localization and caused oscillations reminiscent of anillin-depletion (Beaudet et al. 2017).

Our lab subsequently uncovered a mechanism where Ran controls the localization and function of anillin during cytokinesis through importins (Beaudet et al., 2017; Beaudet et al., 2020). A gradient of importins free to bind NLS-proteins occurs in mitotic cells where they are highest at the cortex and lowest near chromatin. We found that importin-binding to a conserved NLS in the C-terminal C2 domain of anillin is required to facilitate its localization to the equatorial cortex. Mutating this NLS to disrupt importin-binding delayed anillin's cortical recruitment and caused it to localize to a narrower region compared to non-mutant anillin (Beaudet et al. 2017). In addition, we found that the RBD in anillin autoinhibits the C2 domain, and active RhoA is required to relieve this inhibition (Beaudet et al. 2020). Our model is that during anaphase, increased levels of active RhoA promote an open conformation of anillin that is stabilized by importin-binding to increase its accessibility to other components required for its localization to the equatorial membrane (Beaudet et al. 2017; Beaudet et al., 2020). This would ensure that anillin is most robustly recruited away from chromatin to coordinate chromatin with ring position.

The regulation of anillin by importins raises the exciting possibility that Ran could regulate additional cytokinesis proteins. Since thousands of proteins are predicted to have NLSs, it is unlikely that anillin is the only contractile protein regulated by Ran and importins (Nair et al. 2003; Bernhofer et al. 2018). Indeed, other cytokinesis regulators, such as Ect2, Cyk4, and MKLP1, also have NLSs. Whether importin-binding controls the function of these proteins for cytokinesis requires further study.

1.6 Thesis summary

Several questions remained regarding how importin-binding regulates anillin function. In particular, the phenotype caused by the NLS mutation was reminiscent of that caused by the over-extension of microtubules using MCAK-depletion. Further, we mapped the microtubule-binding

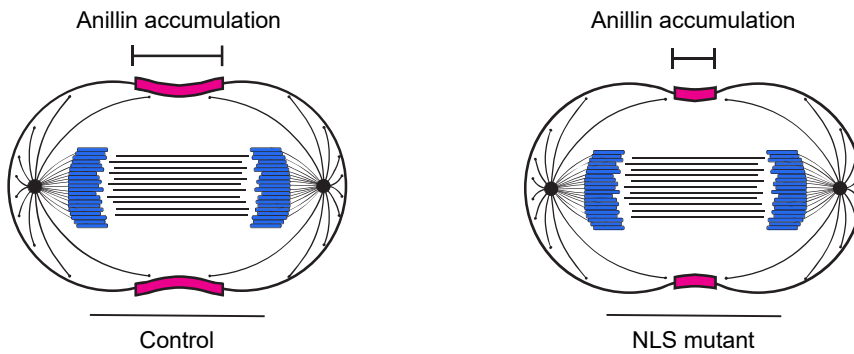
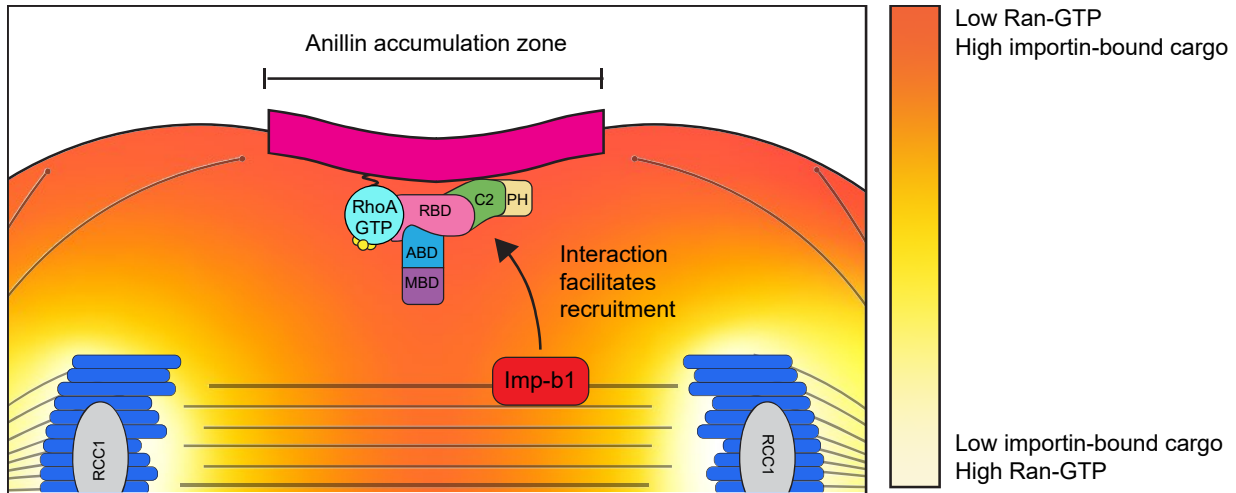


Figure 4. Ran-GTP and importins regulate the recruitment of anillin to the cleavage furrow.

The anchoring of RCC1 (gray) to chromatin (light blue) generates a gradient of active Ran-GTP (blue) in the dividing cell highest near chromatin; this gradient is dynamic, as sister chromatids are segregated in anaphase. The gradient of active Ran establishes an inverse gradient of importins (red), which are bound to Ran near chromatin and free to bind to NLS-proteins away from chromatin. Regions with high Ran-GTP and low importin-bound cargo are in light yellow, and regions with low Ran-GTP and high importin-bound cargo are in orange. In our model, in anaphase, importin-binding facilitates the recruitment of anillin (purple) to the equatorial cortex, away from chromatin and active Ran, where it can bind to RhoA (cyan) and other contractile proteins. Mutating the NLS of anillin narrows its recruitment at the furrow and can cause cells to fail cytokinesis.

domain to the C2 domain, where the NLS is located. Since both require basic residues to mediate interactions, there is a possibility that the sites overlap and/or that introducing mutations into the NLS could structurally alter the microtubule-binding site. It was crucial to elucidate whether the phenotypes that we observed due to the loss of importin-binding vs. affecting microtubule-binding. In this work, we studied how the binding of importins and microtubules to anillin's C2 are coordinated to regulate anillin's function and localization. Using co-sedimentation assays, we determined that importins and microtubules indeed bind at overlapping sites in the C2 domain, and partially compete for anillin-binding. However, the NLS mutations only mildly affect microtubule-binding, which although has lower affinity has similar binding capacity to non-mutant anillin. Further, the results of localization assays suggest that importin-binding regulates a cortical property of anillin that is distinct from microtubules.

We also wanted to elucidate how RhoA and importin-binding are coordinated to regulate anillin function. Previous data showed that the RBD autoinhibits the C2 domain. Since the RBD binds to active RhoA, we proposed that active RhoA binding is required to induce conformational changes that favor importin-binding in the neighbouring C2 domain. Using conditions to increase or decrease the levels of active RhoA, we found that importin-binding indeed was enhanced when levels of active RhoA were high vs. low.

To determine if Ran regulates the function of other cytokinesis proteins, we tested whether the crucial cytokinesis regulator Ect2 is a target of this pathway. Mutating the NLS of Ect2 abrogates its ability to rescue cytokinesis failure in Ect2-depleted cells, suggesting that Ect2 requires an intact NLS for cytokinesis.

Moreover, we performed a proximity-biotinylation assay (BioID) to probe the interactome of importin- β 1 in mitotic cells to identify new targets of the Ran pathway in cytokinesis. Although analysis has revealed that our assay may not have been selective for mitotic cells, we confirmed 32 previously published interactions and identified 206 potential new proximity interactors. These

results hint at a significant and previously unappreciated role for the Ran pathway as a regulatory mechanism of cytokinesis. Elucidating which proteins and how they are regulated by the Ran pathway will resolve the role of this pathway as a regulator of cytokinesis.

Chapter 2: Materials & Methods

2.1 Cell culture

HeLa and HEK293 cells were plated and grown in Dulbecco's Modified Eagle Medium (DMEM; Wisent), supplemented with 10% cosmic calf serum (CCS; Hyclone), and 2 mM L-glutamine (Wisent) and were maintained at 37°C with 5% CO₂. For immunofluorescence microscopy, cells were plated in DMEM media without antibiotics (Penicillin/Streptomycin), and transfected the following day using Lipofectamine 2000 or 3000 (Invitrogen) according to the manufacturer's protocol, except that 3 µL of Lipofectamine was used per 2 mL of media with 0.5–2.0 µg plasmid DNA and 3 µL of 100 µM anillin siRNAs, 2.5 µL of 20 µM Ect2 siRNAs, or 2.4 µL of 100 µM of MCAK siRNAs, as described previously (Yüce et al. 2005; Piekny and Glotzer 2008; Rankin and Wordeman 2010). Cells were imaged 24–26 hours after DNA transfection, and 27–30 hours after co-transfection of DNA and siRNAs. Anillin and Ect2 constructs were used as described previously (Yüce et al. 2005; Piekny and Glotzer 2008; van Oostende Triplet et al. 2014). For *in situ* pull-down assays, cells were lysed 24-hours after DNA transfection. For proximity-based biotinylation, cells were seeded and transfected on the same day and lysates were collected 24-hours after DNA transfection.

2.2 Plasmids

The following plasmids were used in this study. A stable HeLa mCherry:Tubulin cell line was generated previously (van Oostende Triplet et al. 2014). pEGFP-N1:Importin-β was obtained by Addgene, made by Patrizia Lavia (plasmid #106941). GST:Importin-β was made by cloning Importin-β cDNA from the pCMV6-Entry:Importin-β vector (Origene; #RC200659) into pGEX-4T using *NcoI* and *NotI* (New England Biolabs). The anillin constructs for mammalian cell expression

(GFP-tagged) or protein expression (MBP) were generated previously (Piekny and Glotzer 2008; Frenette et al. 2012). The 850KK851-DE or 887KK888-DE (anillin NLS mutant), 735LL736-DD (*strong I/F* mutant) were generated in the anillin constructs by PCR-directed mutagenesis. The Myc:Ect2 (Full-length, C-terminus) constructs were generated previously (Yüce et al. 2005; Frenette et al. 2012). Mutant BirA* and Importin- β or mNeonGreen fusions were made by cloning Importin- β cDNA from the pCMV6-Entry:Importin- β vector or mNeonGreen cDNA from the pNCS-mNeonGreen vector (Allele Biotech) into either C1(1-29)-TurboID-V5_pCDNA3 (plasmid #107173) or C1(1-29)-miniTurboID-V5_pCDNA3 (plasmid #107174) through HiFi assembly homologous recombination (New England Biolabs). TurboID and miniTurboID plasmids (#107173-4) were made by Alice Ting; the C1(1-29) membrane targeting sites was removed from our fusions (Branon et al. 2018). Ect2:mNeonGreen was generated by cloning Ect2 cDNA from pCMV-(myc)3:Ect2 and mNeonGreen cDNA from the pNCS-mNeonGreen vector (Allele Biotech) into pEGFP-N1 via HiFi assembly homologous recombination; EGFP was removed from these constructs. The 347RKRRR351-AAAAA mutations (Ect2 NLS mutant) were generated in the Myc:Ect2 (Full-length) by PCR-directed mutagenesis. All constructs were verified by sequencing.

2.3 Microscopy and immunostaining

Cells were fixed for immunofluorescence using 10% w/v cold trichloroacetic acid (TCA) as described previously (Yüce et al. 2005). Fixed cells were immunostained for, anillin using 1:200 rabbit polyclonal anti-anillin antibodies (Piekny and Glotzer 2008) and myc using 1:250 mouse monoclonal anti-myc antibodies (Developmental Studies Hybridoma Bank). Anti-rabbit or -mouse Alexa 488 and anti-mouse or -rabbit Alexa 568 (Invitrogen) secondary antibodies were used at a 1:250 dilution. DAPI (Sigma-Aldrich) was added at a 1:1000 dilution (1 mg/mL stock) for 5 minutes before mounting the coverslips onto slides. Fixed cells were imaged using a Leica DMI6000B wide-field microscope with the 63x/1.4 PL APO oil immersion objective (pixel size 0.102 μm), and

Z-stacks of 0.5 μm were acquired with a Hamamatsu OrcaR2 camera and Volocity software (PerkinElmer) using a piezo Z stage (MadCityLabs). Image files were exported as TIFFs, which were opened with ImageJ (NIH) and converted into maximum intensity Z-stack projections. Projections and merged colour images were then converted into 8-bit images and imported into Illustrator (Adobe) to make figures.

For rescue assays, threshold levels for rescue were set at a minimum of 1,000 a.u. (arbitrary units) for Myc expression in control and experimental cells using the same imaging settings. Images for figures were processed as composite high-intensity Z-projects or single-channel greyscale high-intensity inverted-colour images for Myc expression in ImageJ (NIH). Projections and merged colour images were then converted into 8-bit images and imported into Illustrator (Adobe) to make figures.

To perform live imaging, media was replaced with phenol red-free DMEM media. Cells were plated and transfected on 25 mm round coverslips (No. 1.5) placed in a 35 mm Chambridge magnetic chamber (Quorum). Cells were kept at 37°C with 5% CO₂ using the INU-TiZ-F1 chamber (MadCityLabs). Live imaging was performed on an inverted Nikon Eclipse Ti microscope with a Livescan Swept Field confocal unit (Nikon), using the 60x/1.4 CFI PLAN APO VC oil immersion objective (pixel size 0.27 μm), a piezo Z stage (MadCityLabs), and with the iXON897 EMCCD camera (Andor). Images were acquired with 200 ms exposures using the 488 and 561 nm lasers (100 mW, Agilent) set between 20–40% power, depending on the intensity of fluorescent signals (settings were kept constant for related experiments based on control cells), and multiple Z-stacks of 0.5 μm were taken every 60 seconds per cell using NIS-Elements acquisition software (Nikon), and a narrow GFP or dual filter (500-544 and 600-665 nm; Chroma). Image files were exported as TIFFs, which were opened with ImageJ (NIH) and converted into maximum intensity Z-stack projections. Projections and merged colour images were then converted into 8-bit images and imported into Illustrator (Adobe) to make figures.

FRAP experiments were performed as in Beaudet et al. 2020. Cells were plated and transfected on 25 mm round coverslips (No. 1.5) placed in a 35 mm ChamSlide magnetic chamber (Quorum). Cells were kept at 37°C with 5% CO₂ using the INU-TiZ-F1 chamber (MadCityLabs). Live imaging and FRAP was performed using a Nikon C2 laser scanning confocal microscope using the 100X Plan Apo I (NA1.4) objective and Elements 4.0 acquisition software (Nikon). Timelapse images were acquired at resolution of 1024x1024 pixels every 2 seconds for a total of 60 seconds. Two time points were acquired prior to photobleaching and for up to 50 seconds after photobleaching. Photobleaching of control and experimental ROI's took place for a total of 5 seconds by pulsing 10 times with the laser power set between 20–50%. Movies were exported as TIFFs then opened with ImageJ (NIH) for analysis. Fluorescence intensity of bleached and non-bleached ROIs were corrected for acquisition bleaching and normalized to background. The average intensity of each ROI was plotted over time using Prism software and the signal recovery rate and maximum recovery of signal was determined using non-linear regression fitting with the following formula:

$$F(t) = y_{max}(1 - e^{-\tau t})$$

Where $F(t)$ describes the fraction of fluorescence recovery for each time point after photobleaching compared to the pre-bleached signal, y_{max} describes the maximum fluorescence recovery after photobleaching, and τ describes the time constant for fluorescence signal recovery. The half-life ($\tau_{1/2}$) or time taken to reach half the maximum fluorescence recovery after photobleaching was determined by the following equation:

$$\tau_{1/2} = \ln(2) / \tau$$

And the immobile fraction was determined as follows:

$$F_{imm.} = 1 - y_{max}$$

Where, F_{imm} is the percent difference between the initial average fluorescence signal before photobleaching and the maximum signal recovered (y_{max}) after photobleaching.

2.4 Rescue assay

Rescue assays were performed as described previously (Piekny and Glotzer 2008). Briefly, cells were co-transfected with Ect2 siRNAs (Dharmacon) to deplete endogenous protein and with either wild-type or NLS mutant (347RKRRR351-AAAAA) Myc:Ect2 plasmid DNA made resistant to RNAi to assay for rescue of the cytokinesis phenotype (e.g. mononucleate vs. binucleate cells). Cells were imaged 24-30 hrs after co-transfection, fixed and immunostained with anti-myc antibodies, anti-anillin antibodies and DAPI as described above. Mononucleate and binucleate cells were counted on ImageJ and data was analyzed by ANOVA and Tukey's post-hoc tests using PSPP.

2.5 Protein purification and pull-downs

The following proteins were made from *E. coli* BL21 cells: GST, GST:Importin- β , MBP, MBP:Anillin (C2; 750-872), MBP:Anillin (RBD + C2; 672-872), and MBP:Anillin (C-term; 608-1087), as well as containing mutations described previously. Bacteria were resuspended in lysis buffer [2.5 mM MgCl₂, 50 mM Tris, 150 mM NaCl pH 7.5, 0.5% Triton X-100, 1 mM dithiothreitol (DTT), 1 mM phenylmethanesulfonyl fluoride (PMSF) and 1 X protease inhibitors (Roche)], incubated with 1 mg/mL lysozyme on ice for 30 minutes, then sonicated three times. Extracts were incubated with pre-equilibrated amylose resin (New England Biolabs), glutathione sepharose 4B (GE Lifesciences) for 5 hours or overnight at 4°C with shaking. After washing, beads were stored as a 50% slurry at 4°C or eluted in equivalent volumes of 100 mM maltose or 10 mM glutathione (pH 8.0) on ice for 2 hours. Protein concentration was determined by running

samples by SDS-PAGE and measuring the density of bands in comparison to known concentrations of BSA (bovine serum albumin) and/or by Bradford assay for eluted proteins.

To test for binding, proteins were pulled down from cell lysates after transfection or using eluted recombinant purified protein. Transfected HeLa cells were lysed in 50 mM Tris pH 7.6, 150 mM NaCl, 5 mM MgCl₂, 0.5% Triton X-100, 1 mM DTT, 1 mM PMSF with 1 X protease inhibitors (Roche) and incubated with 5-10 µg of purified MBP-tagged anillin or GST-tagged importin-β protein on beads at 4°C overnight. Eluted proteins were added to beads at final concentrations as indicated. After binding, beads were washed 3–4 X with 50 mM Tris pH 7.6, 150 mM NaCl, 5 mM MgCl₂ before adding SDS sample buffer to denature the proteins for SDS-PAGE. All samples were run by SDS-PAGE and wet-transferred to nitrocellulose membrane for western blotting. All blots were reversibly stained with Ponceau S to show total protein. The blots were blocked with 5% milk for 20 minutes, then incubated with either mouse anti-MBP antibodies at a dilution of 1:5000 (New England Biolabs) or 1:2500 mouse anti-GFP antibodies (Roche) in 1 X PBS-T (0.140 M NaCl, 2.7 mM KCl, 10 mM Na₂HPO₄, 1.8 mM KH₂PO₄, 0.5% Triton X-100) for 1-2 hours at room temperature. After washing the membrane 3-4 X with 1 X PBS-T, secondary antibodies [anti-rabbit-HRP or anti-mouse-HRP (Cedarlane)] were added as per manufacturer's instructions in 1 X PBS-T for 1 hour. The blots were developed using enhanced chemiluminescence (ECL) western blotting detection reagents (GE Amersham) and visualized on a GE Amersham Imager 600. All results from each pull down assay were replicated in at least three distinct experiments to ensure reproducibility.

2.6 Co-sedimentation assays

Microtubules were prepared from lyophilized microtubules (Cytoskeleton) as per manufacturer's instructions in resuspension buffer (15 mM PIPES, 1 mM MgCl₂, 20 µM Taxol;

Bioshop) at room temperature for 10–15 minutes with gentle mixing. Aliquots of 45.5 μM were flash frozen and stored at -80°C , then thawed in a circulating water bath and diluted with resuspension buffer to 9.1 μM . Purified anillin and importin proteins were pre-spun by centrifugation at 279,000 g for 30 minutes at 25°C . Co-sedimentation reactions were prepared in 200 μL polycarbonate tubes (Beckman Coulter) with 0.5–4 μM of microtubules and 1 μM of purified anillin, or 4 μM of microtubules, 1 μM of purified anillin and 0.2–1.5 μM of purified importin- β , 150 mM NaCl and BRB80 buffer (80 mM PIPES pH 6.8, 1 mM EGTA, 1 mM MgCl_2) containing 1 mM DTT and 10 μM Taxol. The reactions were kept at room temperature for 15 minutes, then centrifuged at 279,000 g for 30 minutes at 25°C . The supernatants were collected, and pellets were washed and re-suspended in BRB80. Sample buffer was added to supernatants and resuspended pellets, which were then run by SDS-PAGE and stained with Coomassie Blue. Scanned gels were analyzed in ImageJ to measure the concentration of proteins using line plots to determine pixel intensities that were imported into Excel (Microsoft). After correcting for background, the average intensity was determined. The average amounts of bound anillin (Y axis) were plotted against free microtubule concentration (X axis) using GraFit version 7.0.3. The apparent dissociation constant (K_D) and binding capacity were determined using non-linear regression (N=3 assays). For the competition assay, after correcting for background, the pixel intensity of anillin in the supernatant was divided by the pixel intensity of anillin in the pellet to obtain a ratio of anillin (S/P) for each concentration of importin- β . Anillin ratios for importin- β concentrations 0.2 – 1.5 μM were compared to control and data was analyzed using the Student's *t* test (two tailed; N=3 assays).

2.7 Proximity-based biotinylation and mass spectrometry analysis

We performed proximity-based biotinylation (BioID) to identify importin- β binding partners during mitotic exit. HEK239 cells were seeded in 100 mm culture plates at 60-70% confluency

and transfected with Importin- β :miniTurbo or mNeonGreen:miniTurbo (Branon et al. 2018). To synchronize cells in metaphase, cells were treated with nocodazole 8 hours-post transfection for 16 hours. Cells were released from nocodazole (50 ng/mL) and fed with biotin (100 μ M; in DMEM) for 30 minutes (15-50 minutes for time-course), then lysed. Cell lysates were collected and clarified by centrifugation at 12,000 g for 3 minutes at 4°C. Protein concentrations of clarified lysates were quantified and equal amounts of total protein for control (transfected with mNeonGreen:miniTurbo) and experimental (transfected with Importin- β :miniTurbo) were incubated with pre-equilibrated streptavidin beads (Sigma-Aldrich) overnight at 4°C with shaking. After binding, beads were washed 3–4 X with 50 mM Tris pH 7.6, 150 mM NaCl, 5 mM MgCl₂ before adding SDS sample buffer and boiling to denature the proteins for SDS-PAGE. A portion of the samples were used to validate expression of the fusion proteins by western blotting using an anti-V5 antibody to detect the V5 epitope tag. Samples were resolved by SDS-PAGE. For time-course biotinylation experiments, polyacrylamide gels were stained with Coomassie Brilliant Blue R-250 (BIORAD) or with silver stain (BIORAD) according to the manufacturer's protocols. For mass spectrometry analysis, polyacrylamide gels were stained with the mass spectrometry-safe stain Simply Blue (Invitrogen) for visualization of protein bands and amounts. Excised gel pieces were reduced with 50 mM NH₄HCO₃, 10 mM DTT for 30 minutes at room temperature, then alkylated with 50 mM NH₄HCO₃ and 50 mM iodoacetamide for 30 minutes at room temperature. Reduced and alkylated gel pieces were washed and dehydrated at room temperature with 50 mM NH₄HCO₃ for 15 minutes, with 25 mM NH₄HCO₃ containing 5% acetonitrile for 15 minutes, with 25 mM NH₄HCO₃ containing 50% acetonitrile for 30 minutes twice, and with 100% acetonitrile for 10 minutes. Dehydrated gel pieces were dried by SpeedVac (Savant) at 43°C and peptides were in-gel digested with proteomics-grade trypsin (Sigma-Aldrich) overnight at 30°C. Digested peptides were extracted from gel pieces and acidified with 60% acetonitrile containing 0.5% formic acid. Extracted peptides were evaporated to dryness by SpeedVac (Savant) at 43°C and stored

at -20°C. Dried samples were resuspended and analyzed using liquid chromatography-tandem MS at Concordia's Centre for Biological Applications of Mass Spectrometry (CBAMS). Liquid chromatography-tandem MS (LC-MS/MS) analyses were performed on a Thermo EASY nLC II LC system coupled to a Thermo LTQ Orbitrap Velos mass spectrometer equipped with a nanospray ion source at positive mode.

2.8 Analysis of mass spectrometry data

Mass spectrometry data was analyzed using the Proteome Discoverer 2.3 software (ThermoFisher Scientific). Tryptic peptide spectra were matched against a database of human proteins. Significant KPNB1 interactors were identified to be proteins with 3 or more unique peptides and having an abundance ratio (KPNB1/mNeonGreen) over 1.00. Proteins with 3 or more unique peptides without a value for abundance ratio were kept if they were present in the KPNB1 experiment and absent from the mNeonGreen experiment. The list of 238 proteins was compared to published interactors of KPNB1 found on the curated database BIOGRID. Functional annotation of the protein dataset was analyzed using DAVID v6.8 (LHRI) with a medium classification stringency and an EASE of 1.0 . Interaction network for 179 proteins was obtained using STRING-db and figure was prepared on Cytoscape and Illustrator (Adobe).

Chapter 3: Results

3.1. The cortical properties of anillin are regulated differently by importins and microtubules

Beaudet et al. (2017) showed that importins regulate anillin's localization. Disrupting this interaction by mutating the NLS in the C2 domain narrows the breadth of anillin at the furrow and impairs its ability to rescue cytokinesis failure. However, the C2 domain of anillin also binds to microtubules, which can modulate anillin's localization. For example, anillin shifts from the membrane to spindle microtubules in cells treated with Taxol, a microtubule-stabilizing drug (van Oostende Triplet et al. 2014). The microtubule-binding domain is in the C2, but has not been precisely mapped (**Figure 5A**). These domains are enriched in basic residues that interact with the acidic tail of alpha/beta-tubulin. Since the NLS also contains basic residues and is in the C2 domain (**Figure 5A**), we determined if the sites overlap, and how the binding of importins and microtubules are coordinated to regulate anillin. We first confirmed that mutating the NLS decreases importin-binding *in vitro* using pull-down assays. While eluted GST:importin- β bound to beads with immobilized MBP:anillin (C2), it failed to bind to MBP:anillin (C2 NLS mutant; 850KK851- DE; **Figure 5B**) or MBP (negative control; **Figure 5C**). Then, we determined if the C-terminal NLS is required for microtubule-binding. To do this, we performed co-sedimentation assays. In these assays, high-speed centrifugation is used to pellet microtubules, and if a protein binds to the microtubules, then it also pellets or co-sediments. Eluted 1.0 μ M MBP:anillin (C2) was added to increasing concentrations of Taxol-stabilized microtubules (0.5 – 4.0 μ M), and centrifuged (**Figure 6A**). The affinity of anillin for microtubules was determined by measuring changes in the intensity of anillin in the supernatant (unbound to microtubules) compared to the pellet (bound to microtubules) on a Coomassie-stained gel. The 'bound' fractions were graphed as a function of microtubule concentration to determine the apparent dissociation constant (K_D)

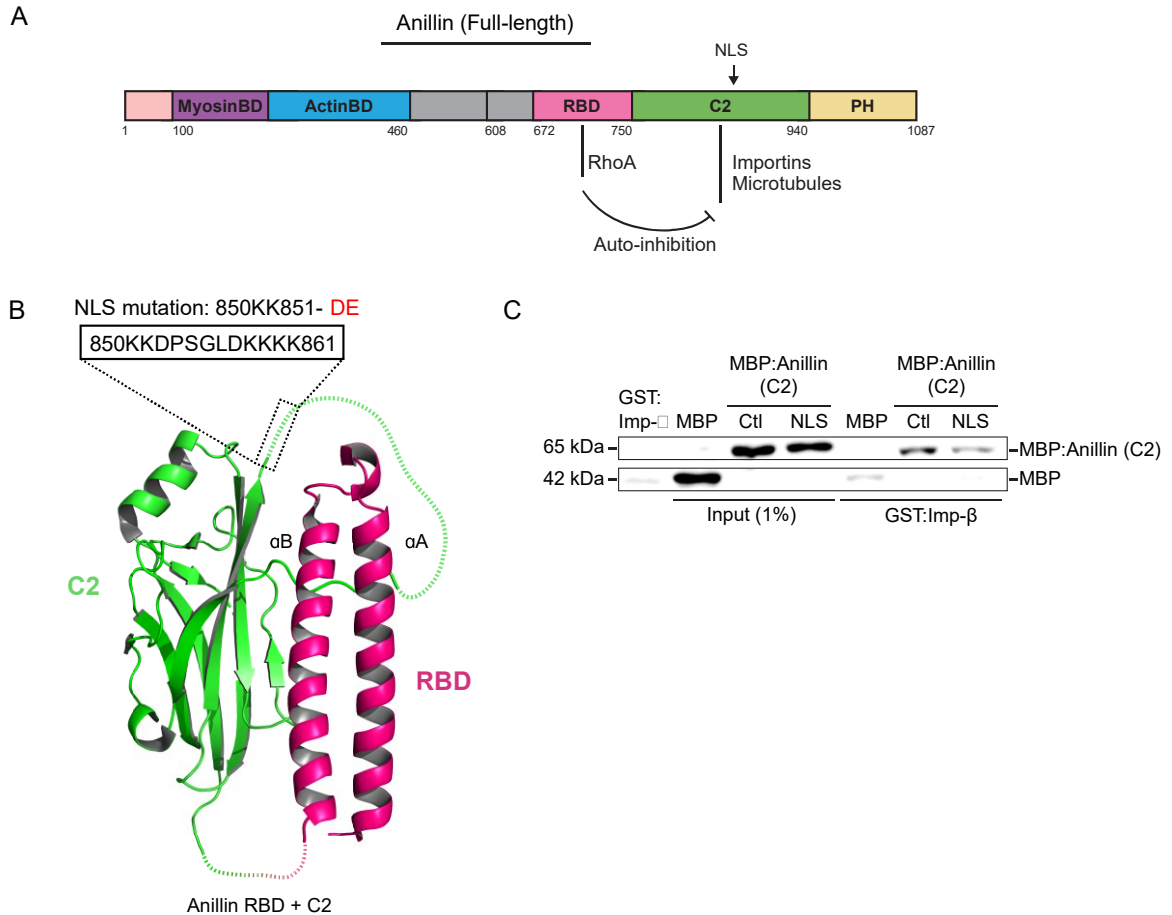


Figure 5. The NLS of anillin is required for importin-binding *in vitro*. (A) The structure of anillin is shown for reference. Importins bind to the NLS in the C2 domain, and microtubules also were shown to bind to the C2 domain, but their precise binding region had not been mapped. (B) A ribbon diagram shows the structure of the RBD and C2 domains of anillin, with the RBD in magenta and the C2 in green. The boxed inset shows the NLS residues and those that were mutated. (C) Images of immunoblots show the *in vitro* binding of GST-tagged importin-β to immobilized MBP, MBP-tagged C2 domain of anillin or with the NLS mutations. Inputs are shown on the left and pull downs on the right.

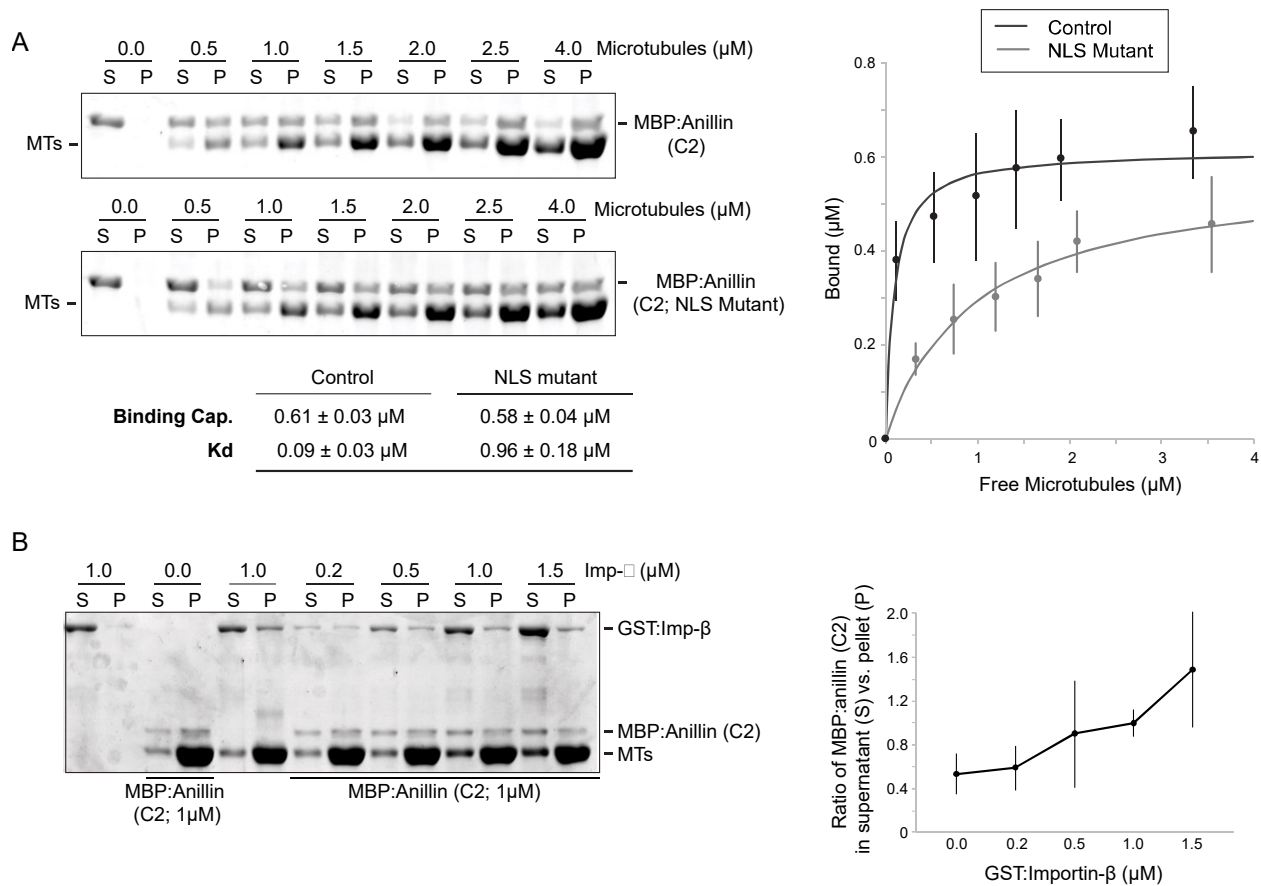


Figure 6. Importin and microtubules partially compete for anillin-binding. (A) Images show coomassie-stained gels with proteins from co-sedimentation assays containing 0 – 4.0 μM purified microtubules (MTs) and 1.0 μM MBP-tagged anillin C2 (top) or NLS mutant (bottom; S, supernatants; P, pellets). The table shows their mean binding capacity and apparent dissociation coefficients (K_D), along with the standard deviation (SD). The graph shows bound anillin C2 (μM; Y-axis) plotted against free microtubules (μM; X-axis). Bars show SD (N=3 replicates). (B) An image of a coomassie-stained gel shows proteins from co-sedimentation assays containing 2.5 μM purified MTs incubated with 1.0 μM MBP-tagged anillin C2 and 0 – 1.5 μM GST-tagged importin-β (S, supernatants; P, pellets). The line graph shows the ratio of anillin (C2) in the supernatant (S) vs. pellet (P) for the indicated concentrations (μM) of GST:Importin-β. Data points show SD (N=3 replicates). Data was analyzed and p values were determined by the unpaired Student's t test (n.s. not significant, * $p < 0.05$). This figure was adapted from Beaudet et al. (2020), used under an Attribution–Noncommercial–Share Alike 3.0 Unported Creative Commons License (CC BY-NC-SA 3.0). Experiments done in collaboration with Daniel Beaudet.

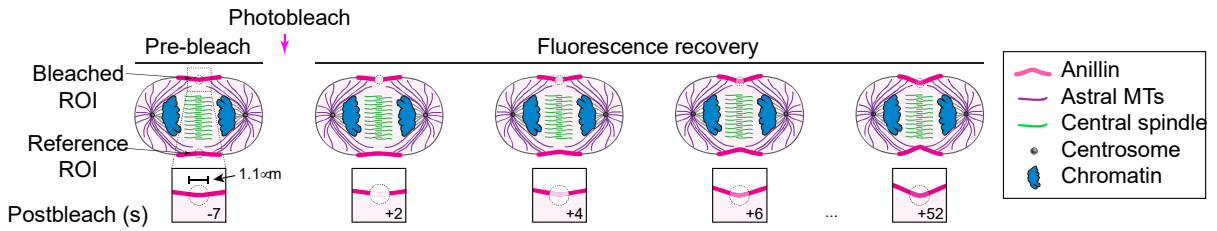
and binding capacity. The apparent K_D was calculated to be $0.09 \pm 0.03 \mu\text{M}$, while the capacity was $0.61 \pm 0.03 \mu\text{M}$ (**Figure 6A**). Mutating the NLS increased the apparent K_D by nearly 10-fold, to $0.96 \pm 0.18 \mu\text{M}$, however the capacity, $0.58 \pm 0.04 \mu\text{M}$, was similar (**Figure 6A**). This weaker affinity for microtubules indicates that the region containing the NLS may overlap with the microtubule-binding domain. However, since microtubules can still reach a similar binding capacity this site is not entirely overlapping. Alternatively, the sites may not overlap, since the mutations in the NLS introduce charge changes, this could cause shifts in the structure of nearby helical regions.

Given that there could be potential overlap or structural influence between the importin- and microtubule-binding domains, we tested whether importins and microtubules compete or cooperate for anillin binding. We performed a competition co-sedimentation assay using a fixed concentration of eluted MBP:anillin (C2; $1.0 \mu\text{M}$) and microtubules ($2.5 \mu\text{M}$), with increasing concentrations of eluted GST:importin- β ($0.2 - 1.5 \mu\text{M}$; **Figure 6B**). The change in anillin intensity in the supernatant (unbound to microtubules) compared to the pellet (bound to microtubules) was determined as a ratio and graphed as a function of GST:importin- β concentration (**Figure 6B**). As the concentration of importin- β increased, the ratio of anillin in the supernatant vs. the pellet increased, indicating that anillin was competed from microtubules by importin- β (**Figure 6B**). However, importins did not completely abolish anillin binding to microtubules, suggesting that there is only partial competition between importins and microtubules for anillin-binding, and supports that their binding sites partially overlap.

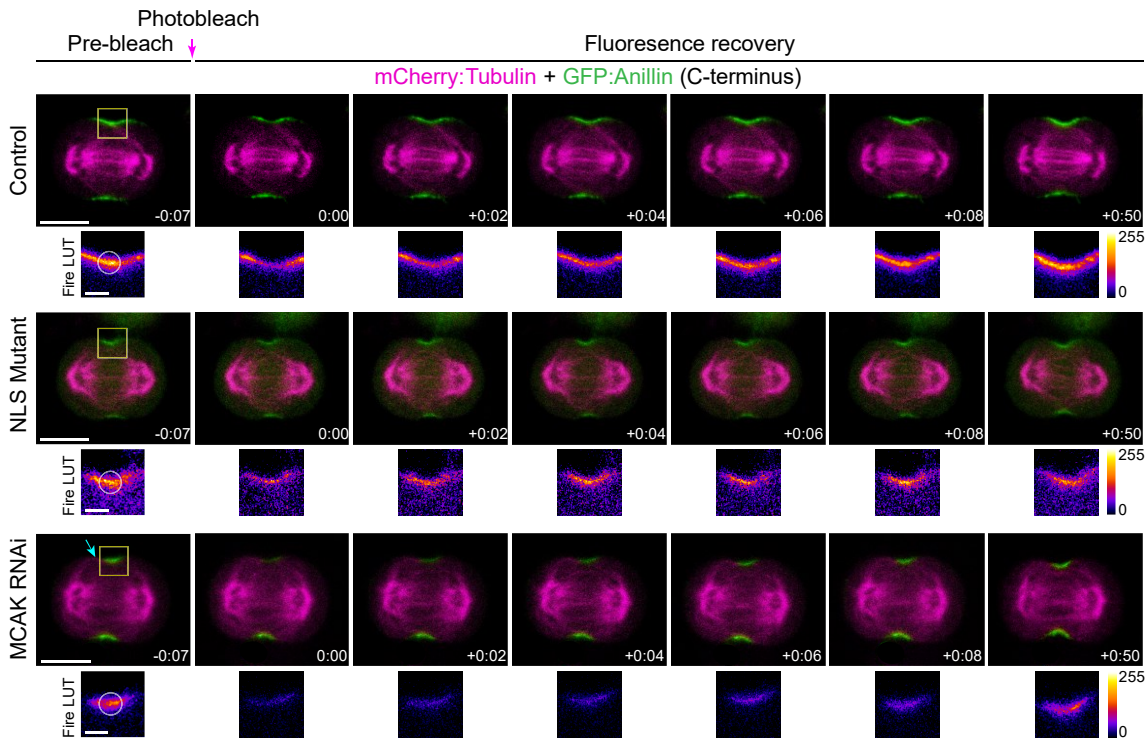
Prior studies showed that astral microtubules restrict the localization of anillin. As mentioned above, anillin localization was observed to shift from the membrane onto Taxol-stabilized microtubules, suggesting competition between these two locations (van Oostende Triplet et al. 2014). This was supported by experiments where over-extending astral microtubules by the RNAi-mediated knock down of MCAK, an enzyme required for microtubule

depolymerization, narrowed the breadth of anillin localization in the equatorial plane (van Oostende Triplet et al. 2014). We observed a similar impact on anillin localization with the NLS mutant of anillin, which was restored when astral microtubules were disrupted (Beaudet et al. 2017). Although the importin- and microtubule-binding regions may overlap, mutating the NLS reduced microtubule-binding affinity, but the capacity was not altered. Thus, the change in anillin localization with the NLS mutations could be due to decreased membrane localization, which could favour restriction by astral microtubules despite the lower affinity. This model would require that the NLS mutant confers different cortical properties that strongly resemble those caused by the over-extension of astral microtubules. To test this, we performed fluorescence recovery after photobleaching (FRAP) experiments on cells co-expressing mCherry:tubulin (to visualize the mitotic spindle) and GFP:anillin (C-terminus; C-term), and compared the fluorescence recovery of anillin, NLS mutant anillin, and anillin in MCAK-depleted cells where astral microtubules were overextended. In these experiments, a region of interest (ROI) on one side of the dividing cell was photobleached, while an ROI on the other side was used as a reference (**Figure 7A**). Timelapse images of cells and their bleached ROI's showed that the C-terminus of anillin recovered quite rapidly at the equatorial membrane, and to an extent that was similar to control. This was particularly evident via the Fire LUTs, which show different colours corresponding to protein levels, where yellow is high, and purple is low, with red in between (**Figure 7B**). The NLS mutant anillin and anillin in MCAK RNAi cells did not recover to the same extent as control cells (**Figure 7C**). Quantification of the % recovery, which was plotted as a function of time for average values, revealed that while anillin recovered (y_{max}) to 98.1%, both the NLS mutant (73.6%) and MCAK-depletion (77.2%) did not (**Figure 7C**). However, how quickly they recovered (τ and $\tau_{1/2}$) differed. While MCAK-depletion did not significantly change the fluorescence recovery time constant (τ) and the half-life ($\tau_{1/2}$) compared to control (0.167 vs. 0.148 and 4.14 vs. 4.67, respectively), the NLS mutant recovered faster and had a shorter half-life (0.323 and 2.15; **Figure 7C**). Thus, the loss of importin-binding by mutating the NLS could increase microtubule's ability to change anillin

A



B



C

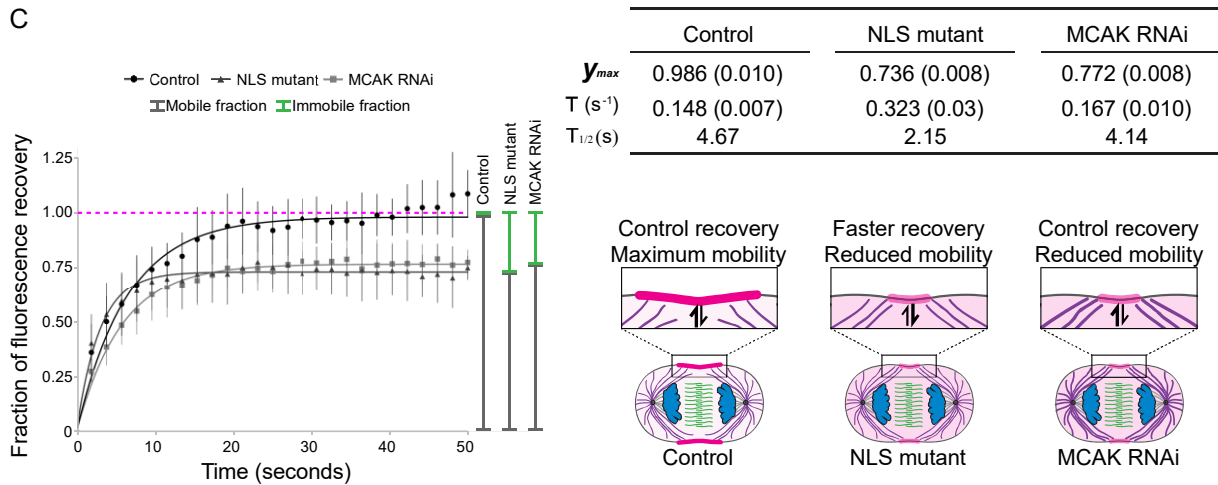


Figure 7. Importins and microtubules regulate distinct cortical properties of anillin. (A) Cartoon schematics show the fluorescence recovery after photobleaching (FRAP) of a region of interest (ROI) compared with a reference ROI in a cell expressing anillin during anaphase and early ingression. The photobleached region is shown in the boxed inset. Other components of the cell are indicated in the legend. (B) Time-lapse images show FRAP of HeLa cells expressing mCherry:tubulin (magenta) and GFP-tagged C-terminus of anillin (green), or with the NLS mutations, or after treatment with MCAK RNAi. The boxed insets show the ROIs that were photobleached in Fire LUTs. The scale bars are 10 or 2 μm for boxed insets. The blue arrow points to overextended microtubules. Indicated times are before (-) or after (+) photobleaching. (C) A graph shows the fraction of fluorescence recovery (*y*-axis) over time (*x*-axis; seconds) for control (*n* = 15), NLS mutant anillin (*n* = 12), or after MCAK RNAi (*n* = 8). The green lines indicate the immobile fraction, while the gray lines show the mobile fraction. Bars show SD. The table shows the maximum recovery (y_{max}), fluorescence recovery time constant (τ), and half-life ($\tau_{1/2}$) for each condition as indicated. SEM are shown in parentheses. Below the table, cartoon schematics of cells show how mutating the NLS causes a faster recovery vs. MCAK RNAi, which recovers similar to control. However, both the NLS mutant and MCAK RNAi have reduced mobility. This figure was adapted from Beaudet et al. (2020), used under an Attribution–Noncommercial–Share Alike 3.0 Unported Creative Commons License (CC BY-NC-SA 3.0). FRAP experiments were performed by Daniel Beaudet.

localization by causing a pool to shift to an immobile fraction, similar to over-extending astral microtubules. However, the rapid kinetics caused by the NLS mutant suggests that loss of importin-binding causes a distinct change in anillin's affinity for the membrane.

3.2. RhoA and importins feedback to recruit anillin to the cortex

Previous experiments with the C-terminus of anillin showed that the C2 domain is intramolecularly inhibited by the RBD. The C-terminus of anillin did not localize to the nucleus of interphase cells, but removal of the RBD allowed the smaller fragment to localize to the nucleus, which showed that the NLS in the C2 domain was indeed functional (Beaudet et al. 2017). In pulldown assays using cell lysate, the C2 domain pulls down more GFP-importin- β than the RBD+C2 fragment, and in co-sedimentation assays, more C2 is co-sedimented with microtubules than larger fragments containing the RBD (Beaudet et al. 2017). We confirmed that that this auto-inhibition persists *in vitro* with a pulldown assay using purified GST-tagged importin- β or GST on beads with eluted MBP-tagged anillin (C2 or C-term). As expected, the C2 pulled down significantly more importin- β than the C-term (**Figure 8A**).

Building on this work, we posited that the binding of active RhoA to the RBD relieves auto-inhibition of the C2 domain, making it more accessible to importin-binding. RhoA is a small GTPase that is active in its GTP-bound state and inactive in its GDP-bound state. If binding to RhoA stabilizes anillin in a conformation accessible for importin-binding, then we predict that increasing the levels of RhoA-GTP in a cell would lead to increased binding between anillin and importin. We performed a pulldown assay using immobilized purified MBP-tagged anillin (RBD+C2) or MBP to pull down GFP-tagged importin- β from the lysate of cells where we either overexpressed the C-terminus of Ect2 (the RhoGEF activator of RhoA) to increase active RhoA

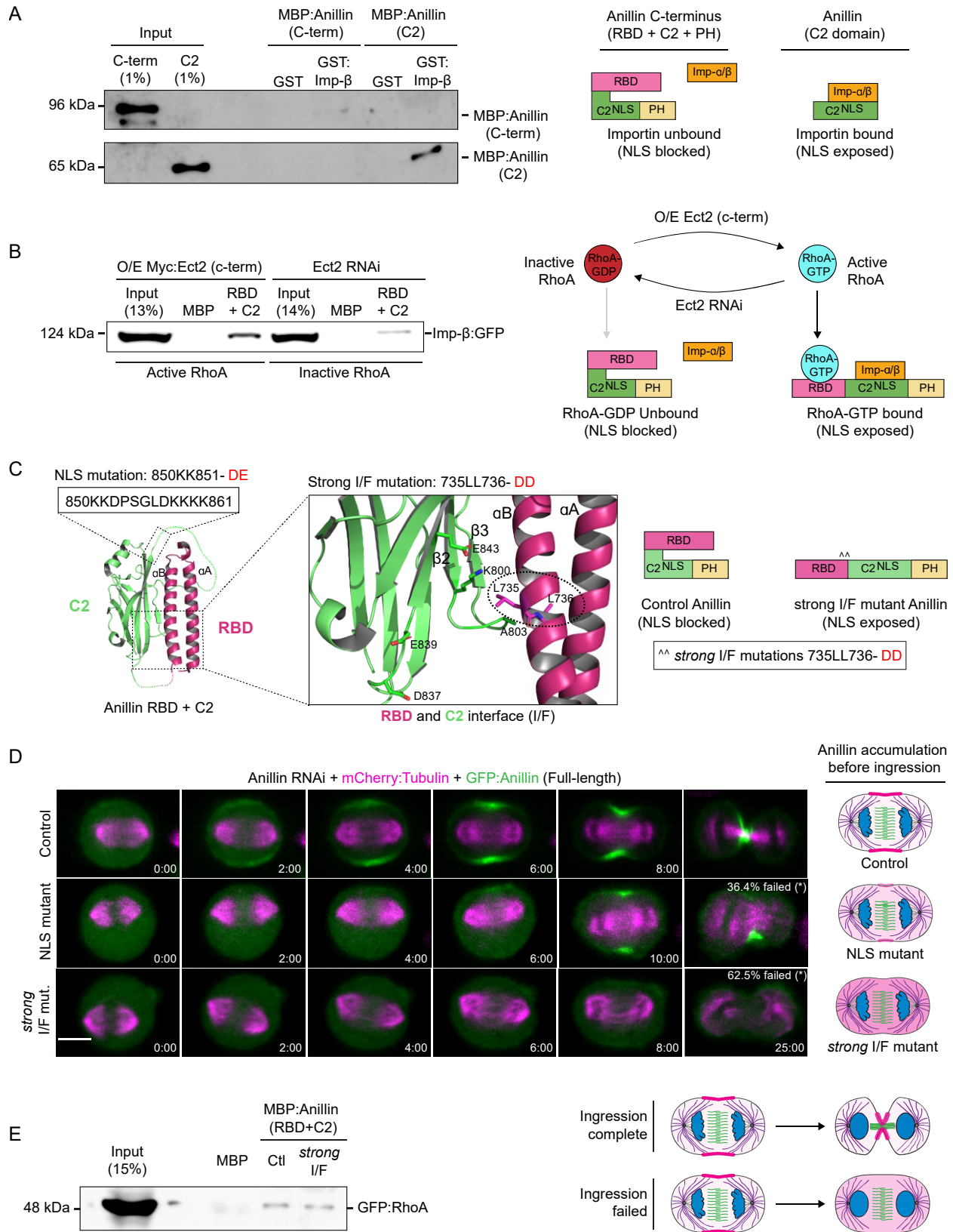


Figure 8. Anillin requires RhoA-binding, importin-binding and the interface between the RBD and C2 for its localization and function in cytokinesis. (A) Immunoblots show *in vitro* binding of purified GST or GST-tagged importin- β (Imp- β) with MBP-tagged C-terminus of anillin (C-term; top) or the C2 domain (bottom). A cartoon schematic shows how the C-terminal NLS within the C2 domain (green) is exposed for importin binding (orange) in the absence of the RBD domain (magenta; PH domain in yellow). (B) An immunoblot shows pull downs of GFP-tagged importin- β from lysates from cells overexpressing (O/E) Myc-tagged Ect2 C-terminus to generate active RhoA (left), or after Ect2 RNAi to reduce active RhoA (right), with purified MBP or MBP-tagged anillin (RBD + C2). Cartoon schematics show how active RhoA (RhoA-GTP) or inactive RhoA (RhoA-GDP) impact anillin's affinity for importins. (C) A ribbon structure shows the intramolecular interface between the RBD (magenta) and the C2 domain (green). In the boxed inset above, the amino acids of the NLS and those that were mutated (850KK8510-DE) are shown in a box. On the right, a boxed inset shows the amino acids that form electrostatic and hydrophobic interactions at the interface. The amino acids that were mutated to generate a *strong* I/F mutant are positioned in the α B helix and are circled (L735D; L736D). The amino acids that mediate RhoA binding map to the α A and α B helices and are positioned away from the C2 domain. To the right is a cartoon schematic illustrating how *strong* I/F mutations are predicted to disrupt the structure of anillin. (D) Time-lapse images show HeLa cells treated with anillin RNAi to deplete endogenous anillin and expressing various RNAi-resistant GFP-tagged full-length anillin constructs (green) and mCherry:tubulin (magenta) as indicated: control ($n = 15$), NLS mutant ($n = 22$) and *strong* interface mutant anillin (*strong* I/F mutant; $n = 16$). Times are indicated from anaphase onset. The scale bar is 10 μ m. For each condition, the percentage of cells that failed ingression are shown. The data were analyzed using two-tailed Fisher's exact test (n.s., not significant; *, $p < 0.05$; ***, $p \leq 0.0001$). To the right and below are cartoon schematics illustrating changes in localization and cells that have completed vs. failed ingression. (E) Immunoblots show pull downs of GFP-tagged RhoA from lysates with MBP or MBP-tagged anillin (RBD + C2), either control (Ctl) or *strong* I/F mutant. This figure was adapted from Beaudet et al. (2020), used under an Attribution–Noncommercial–Share Alike 3.0 Unported Creative Commons License (CC BY-NC-SA 3.0). Live-imaging was performed and models were drawn by Daniel Beaudet.

or depleted Ect2 using siRNAs to reduce active RhoA. MBP-tagged anillin (RBD+C2) pulled down more GFP-tagged importin- β when active RhoA was presumably high compared to when active RhoA was low. This supports our model that active RhoA induces a conformational change in anillin that enhances the importin interaction (**Figure 8B**).

We next sought to determine whether mutations impacting the RBD-C2 interface have an effect on cytokinesis. We generated mutations designed to disrupt hydrophobic interactions in the RBD-C2 interface of anillin to weaken the binding between the RBD and the C2 (**Figure 8C**). This mutant, referred to as the *strong* I/F mutant (735LL736- DD), was shown to partially restore nuclear localization (64% of cells), indicating that it partially relieves the autoinhibition by the RBD (Beaudet et al. 2020). Using time-lapse imaging, we filmed dividing cells depleted of endogenous anillin and co-expressing mCherry-tagged tubulin (to visualize the mitotic spindle) and RNAi resistant GFP-tagged anillin, comparing control, NLS mutant, and *strong* I/F mutant (**Figure 8D**). Cells were imaged starting at anaphase onset when the sister chromatids begin to segregate. In control cells, anillin localizes to the equatorial cortex shortly after anaphase onset, where it remains throughout cytokinesis (**Figure 8D**). As expected, all control cells successfully divided. Delays in anillin recruitment were observed for the NLS mutant and 36.4% of cells failed cytokinesis. As reported in Beaudet et al. (2017), the NLS mutant exhibited a narrower breadth of localization. The *strong* I/F mutant did not localize to the equatorial cortex, and 62.5% of cells failed cytokinesis. These results highlight both the importance of the RBD-C2 interface and importin-binding for anillin recruitment to the contractile ring. To ensure that RhoA-binding was not perturbed by the 735LL736- DD mutations, we performed a pulldown assay with purified MBP-tagged anillin or MBP on beads and GFP-tagged RhoA from cell lysate. The *strong* I/F mutant pulled down similar levels of RhoA as control (**Figure 8E**). Therefore, the inability of this mutant to rescue cytokinesis and localize to the membrane is unlikely to be caused by a change in RhoA-binding per se. Rather, we suggest that in cells the RBD and C2 domain need to bind

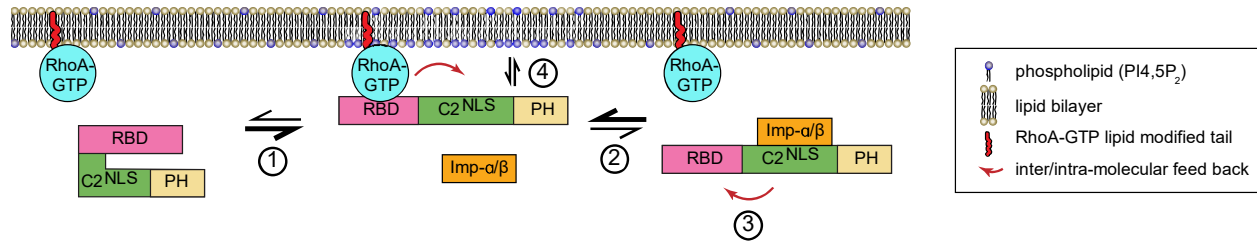


Figure 9. A model for how importin-binding facilitates the RhoA-mediated recruitment of anillin to the membrane during cytokinesis. (1) RhoA is activated (blue) at anaphase onset and binds to the RBD (magenta), which increases anillin's affinity for importin by causing conformational changes between the RBD and the C2 domain (green). (2) Importin-β (orange) binds to anillin via the C-terminal NLS, which (3) feeds back by stabilizing a conformation that enhances cooperative binding of RhoA to the RBD and phospholipids to the C2, which outcompete importin-β (4) for anillin's enrichment at the equatorial cortex. This figure was adapted from Beaudet et al. (2020), used under an Attribution–Noncommercial–Share Alike 3.0 Unported Creative Commons License (CC BY-NC-SA 3.0). Model was drawn by Daniel Beaudet.

cooperatively to RhoA and phospholipids, respectively, for anillin's membrane localization, and the enhanced importin-binding in the mutant fails to hand-off to phospholipids. Thus, we propose that the binding of RhoA induces conformational changes in anillin to relieve autoinhibition of the C2 domain, which is stabilized by importin-binding to facilitate binding to the phospholipids for its membrane recruitment (**Figure 9**).

3.3. Ect2 as a potential target of the Ran pathway during cytokinesis

Ect2 is a GEF for RhoA and a crucial regulator of cytokinesis, but its regulation is not well-understood. As described in the introduction, during metaphase, the N-terminal BRCT domains autoinhibit the C-terminal DH/PH domains, which are required for GEF activity. This is proposed to occur via the binding of the N-terminal BRCT domains to Cdk1-phosphorylated T342, which is in the adjacent S-loop. Interestingly, this residue lies close to a classical bipartite NLS that was previously shown to be important for Ect2's transformation activity (**Figure 10A**; Saito et al., 2004). A recent study showed that T342 phosphorylation inhibits importin-binding, which the authors proposed is required to block nuclear import so that Ect2 is retained in the cytosol during early stages of mitosis (Suzuki et al. 2015). The current model for how autoinhibition is relieved is 1) T342 phosphorylation is lost as cells enter anaphase and Cdk1 activity drops, and 2) the binding of Cyk4, which is phosphorylated by Plk1, to the BRCT domains. Together, these events would induce conformational changes in Ect2 to make the C-terminus accessible to RhoA (**Figure 10B**). We propose that importin-binding via the NLS could facilitate Ect2's activation by inducing and/or stabilizing the open conformation (**Figure 10C**).

To determine if importin-binding is required for Ect2's function during cytokinesis, we mutated several residues in the NLS (347RKRRR351 – AAAAA) and performed a rescue assay (**Figure 11A-B**). We depleted endogenous Ect2 in a population of asynchronous HeLa cells, and

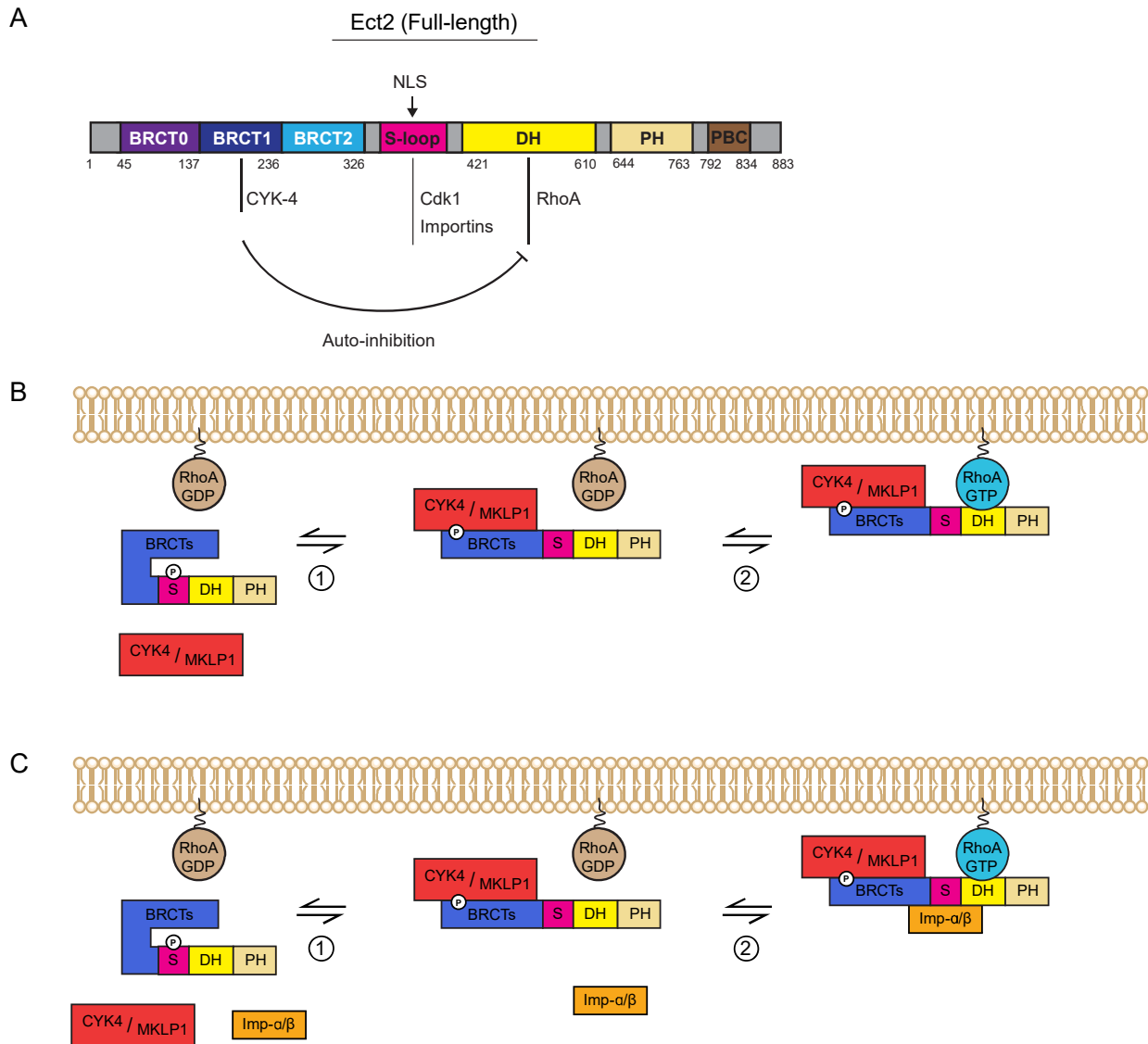


Figure 10. A conformational change in Ect2 is required for its activity. (A) A cartoon shows the structure of Ect2, with the NLS in the S-loop and the auto-inhibition of the C-terminus via the BRCTs. The various binding domains are indicated. (B) A cartoon model shows Ect2 regulation: (1) Cdk1-phosphorylation of T342 in the S-loop autoinhibits the C-terminus in metaphase, and the loss of this phosphorylation combined with the binding of phosphorylated CYK-4 (in a complex with MKLP1) relieves the auto-inhibition of Ect2, and holds it in an “open” conformation; (2) Ect2 is in a favourable conformation to interact with RhoA at the membrane and activate it for cytokinesis. (C) A cartoon model shows how importins could regulate Ect2: (1) the loss of phosphorylation would permit importin-binding, and either CYK-4/MKLP1 binds as in (B), and (2) importin-binding stabilizes the “open” conformation, or importin-binding facilitates CYK-4/MKLP1 binding to induce the “open” conformation (not shown).

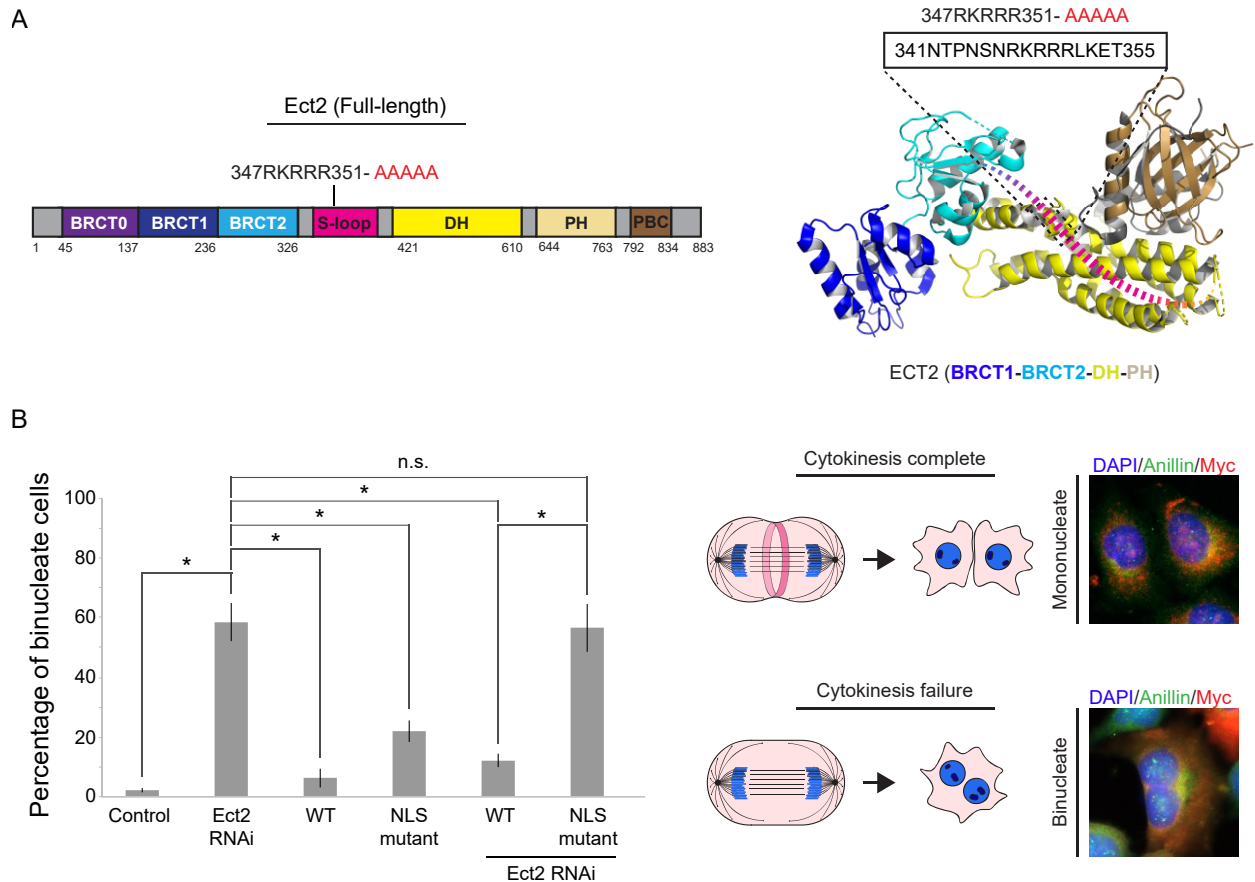
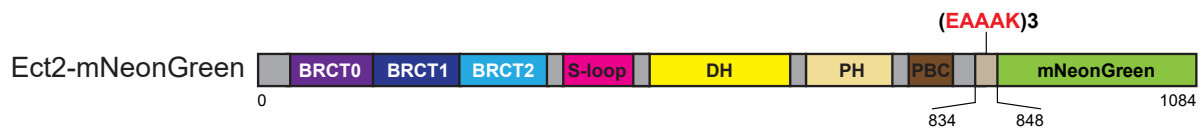


Figure 11. The NLS of Ect2 is required for its function during cytokinesis. (A) On the left, a cartoon structure shows the domains of Ect2 with the mutated residues in the NLS of the S-loop. On the right, the Ect2 ribbon structure is shown, with a boxed inset with the NLS sequence, and the mutated residues are indicated above. (B) On the left, a bar graph shows the percentage of binucleate cells (Y-axis) as a readout of cytokinesis failure in populations of asynchronous HeLa cells after various treatments as indicated on the X-axis. Cells were either not treated (control), or transfected with Ect2 RNAi +/- RNAi-resistant wild-type Ect2 (WT) or NLS mutant Ect2 (347RKRRR351- AAAAA) constructs. Bars show SEM (N = 3 replicates, with n = 20-175 cells counted per condition for each replicate). The data was analyzed using ANOVA and a Tukey's post-hoc test (n.s., not significant; *, $p < 0.05$). On the right, cartoons show cells completing or failing cytokinesis. Images show fixed HeLa cells stained for DNA (DAPI; blue), anillin (green) and Ect2 (Myc for myc-tagged Ect2; red). The top panel shows mononucleate cells that successfully completed cytokinesis, while the bottom panel shows a binucleate cell that failed cytokinesis. Experiments performed in collaboration with Joseph Del Corpo.

co-expressed RNAi-resistant wild-type or NLS mutant myc-tagged Ect2, and then counted the percentage of binucleate cells as a readout for cytokinesis failure (**Figure 11B**). Since cytokinesis occurs after chromosome segregation when it fails the chromatin re-form as two independent nuclei in a single daughter cell (**Figure 11B**). As expected, very few binucleate cells were observed in control cells with no treatment, whereas 53.5% of cells were binucleate when Ect2 was depleted (**Figure 11B**). Although the expression of wild-type Ect2 significantly rescued Ect2-depletion (11.0% binucleate, $p < 0.05$), the NLS mutant was unable to rescue (51.7% binucleate; n.s.), and the proportion of binucleate cells was similar to Ect2-depletion (**Figure 11B**). These data suggest that the NLS is required for Ect2's function during cytokinesis.

We observed that the over-expression of NLS mutant Ect2 caused an increase in cytokinesis failure (19.9% binucleates) in the presence of endogenous Ect2 (**Figure 11B**). This suggests that there could be some dominant-negative effects caused by this construct. A previous study showed that the over-expression of an N-terminal fragment of Ect2 caused cytokinesis defects, suggesting that there is the potential for dominant-negative phenotypes when levels are not carefully controlled (Chalamalasetty et al. 2006). Interestingly, cytokinesis occurred normally with an N-terminal fragment containing the NLS, but defects were observed when the NLS was mutated (Chalamalasetty et al. 2006). Thus, there is a precedent for the NLS sequences to regulate Ect2's function for cytokinesis. The model proposed by the authors of this previous study suggested that transporting Ect2 back to the nucleus is essential to remove it from the contractile ring for successful midbody formation, but we hypothesize that there could be additional regulation of Ect2 function via importin-binding.

To study the role of the NLS for Ect2's function during cytokinesis requires live imaging studies using probes. Ect2 has been challenging to image via over-expressed probes, which are silenced or only very weakly expressed. We were able to overcome this issue by fusing the fluorescent protein mNeonGreen, a yellow-green fluorescent protein from *Branchiostoma*



Ect2 RNAi + Hoechst 33342 + Ect2:mNeonGreen (Full-length)

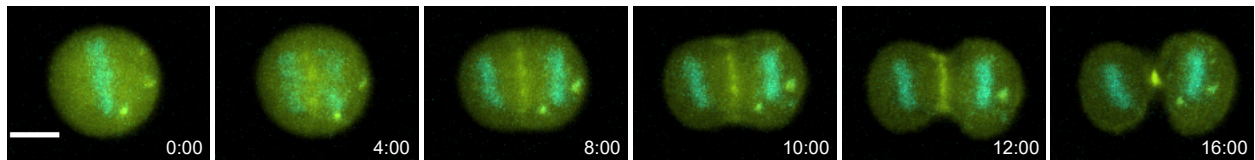


Figure 12. Time-lapse microscopy of Ect2-mNeonGreen in a dividing HeLa cell. A cartoon schematic shows the structure of Ect2 with the mNeonGreen fusion. Below, time-lapse images show a representative HeLa cell depleted of endogenous Ect2 and transfected with mNeonGreen-tagged Ect2 (green) and treated with Hoechst to visualize DNA (blue). Times are shown in minutes, and the scale bar is 10 μ m.

lanceolatum, which is 2.5x brighter than GFP, to the C-terminus of Ect2 separated by a linker [(EAAAK)₃]. Expression of this construct in HeLa cells shows a localization pattern consistent with what has been observed with antibodies to endogenous Ect2 (Tatsumoto et al. 1999; Yüce et al. 2005; Frenette et al. 2012; **Figure 12**). Ect2 localizes to the spindle midzone shortly after anaphase onset, and is both at the furrow and on the midzone during ingression, and finally localizes to the midbody (**Figure 12**).

3.4 Identifying new targets of the Ran pathway during cytokinesis

Work done in our lab has shown that importin-binding is required for anillin's cortical recruitment and function during cytokinesis, and our preliminary data suggests that importin-binding could be important for Ect2 function. Since several core cytokinesis regulators have NLS sequences, this led us to hypothesize that other cortical proteins could be regulated by importin-binding for cytokinesis. To identify potential targets of the Ran pathway in anaphase, we performed a proximity-based biotinylation assay (BioID) using importin- β 1 (KPNB1) as a bait protein in synchronized HEK 293 cells. Importantly, the Ran pathway was already known to regulate mitotic proteins required for spindle assembly. We used long-term treatments of Nocodazole, a microtubule depolymerizing drug, to arrest cells in mitosis, then released them for 30-40 minutes to exit mitosis and enter anaphase (**Figure 13A**). Biotin was added during the release to label proteins that interact with importin- β 1 during mitotic exit. To do short-term treatments of biotin required the use of an improved mutant biotin ligase (BirA*) called "miniTurbo", which allowed us to reduce the biotinylation time from multiple hours in conventional BioID to 30 minutes (Branon et al. 2018). To control for non-specific interactions, we also performed BioID with a fusion of the fluorescent protein mNeonGreen and miniTurbo. Interactions were considered significantly enriched for importin- β 1 vs. mNeonGreen if: 1) protein abundance

(as analyzed by the Proteome Discoverer 2.3 yielded an abundance ratio (importin- β 1/mNeonGreen) was over 1.00, and 2) three (3) or more unique peptides of the protein were detected. A protein was also considered a significant proximity interactor if it was found exclusively in the importin- β 1 data set and for which three (3) or more unique peptides were detected.

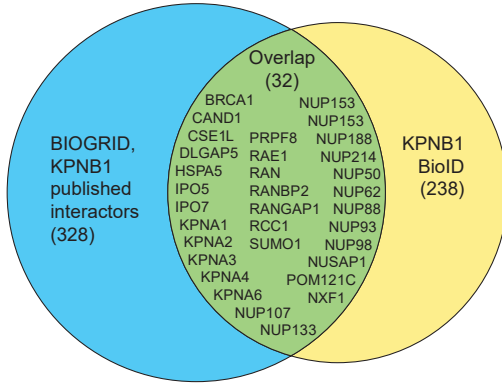
Filtering the list of proteins obtained through mass spectrometry yielded a list of 238 potential proximity interactors. Comparing our data set with a list of published interactors of importin- β 1 from BIOGRID (determined by affinity purification/mass spectrometry, yeast two hybrid, FRET, proximity-label/mass spectrometry, etc.) revealed 32 proteins in common (Oughtred et al. 2019; **Figure 13B**; **Table 1**). The majority of these proteins are involved in nucleocytoplasmic transport, most of them being either importins or nuclear pore complex proteins. As shown in Table 1, most of these proteins were highly enriched in the importin- β 1 data set, with only 5 of them having an abundance ratio < 2.00, and 10 of them being exclusive to the importin- β 1 data set. This overlap with BIOGRID and high enrichment validates the quality of our BioID assay, which identified 206 potential new proximity interactors.

Using the gene functional annotation tool DAVID, clustering these potential proximity interactors by biological process revealed that the data set was enriched for cell adhesion proteins (ES=25.39) and nuclear import proteins (ES=13.02; Huang et al. 2009a; Huang et al. 2009b; **Figure 13C**). Proteins involved in cell division were modestly enriched (ES=3.58). The importin- β 1 proximity interactome was graphically classified using STRING-db and Cytoscape and organized into the following functional clusters: cytoskeletal organization, vesicular transport, cell-cell adhesion, DNA-related processes, translation, nucleocytoplasmic transport and other, with overlap for cell division and cell adhesion shown as additional clusters (Szklarczyk et al. 2019; **Figure 13D**). As with DAVID analysis, this annotation revealed that our BioID assay identified

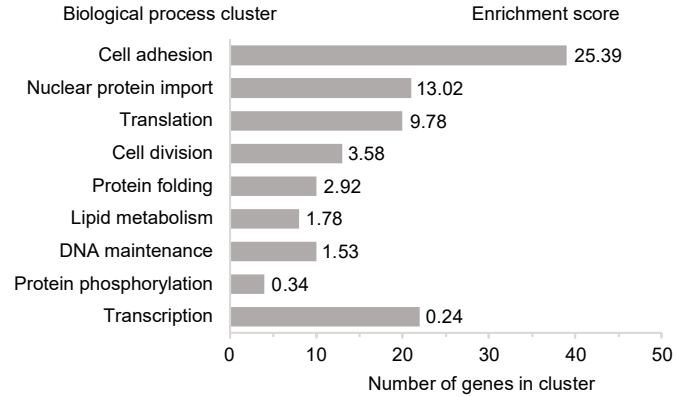
A



B



C



D

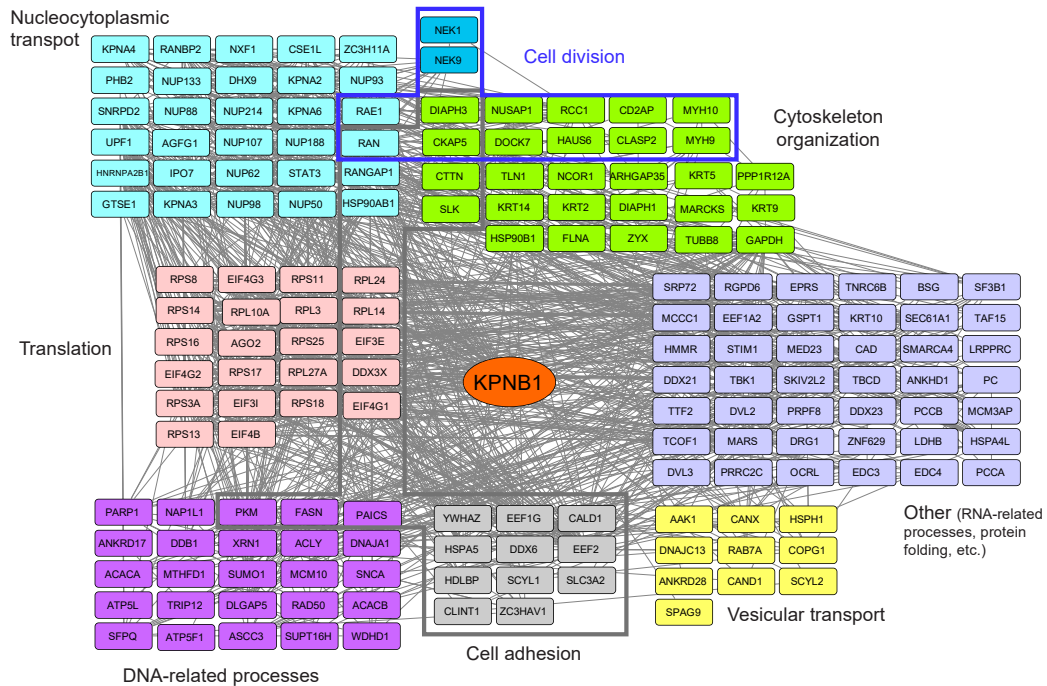


Figure 13. Identification of the importin- β 1 proximity interactome in mitosis using BioID.

(A) The experimental design is shown. HEK 293 cells were seeded and transfected with either Importin- β :miniTurbo or mNeonGreen:miniTurbo at 0 hours. After 6 hours, cells were synchronized to be in metaphase by treating with nocodazole (50 ng/mL), then released at 22 hours by washing with PBS and biotin (100 μ M) was added for 30 minutes. Lysate was collected for the purification of biotinylated proteins using streptavidin beads. Purified proteins were subsequently separated by SDS-PAGE, trypsin-digested and prepared for mass spectrometry. (B) A venn diagram shows the KPNB1 (Importin- β) dataset and published KPNB1 interactors obtained from the curated database BIOGRID. (C) A graph shows the functional annotation of clusters related to biological processes for the KPNB1 BioID dataset. KPNB1 proximity interactors were clustered using the online database “DAVID” (v6.8). Cluster enrichment scores are shown on the right. (D) A schematic shows 179 of 238 KPNB1 potential proximity interactors. Data was analyzed using Cytoscape 3.8.0 with the STRING-db application. Nodes represent potential proximity interactors identified and categorized by biological process based on Gene Ontology information. Light grey edges represent protein-protein interactions from STRING with interaction score of 0.4 or higher. Experiments performed in collaboration with Su Pin Koh.

mostly transport and cell adhesion proteins. It is important to note that most of the proteins we are interested in would fall into the cytoskeletal organization or cell-cell adhesion categories rather than cell division or mitotic proteins, which tend to be dedicated to processes such as centrosome maturation, spindle assembly, chromosome congression, alignment and segregation, among others. While encouraging, these proteins likely reflect early cortical changes during mitotic exit vs. later anaphase or early telophase when there is a greater enrichment of cytokinesis proteins.

Table 1. Importin-β1 interactors common to BIOGRID are enriched in the experimental BioID dataset.

Gene name	Protein names	# Unique peptides	Abundance (KPNB1)	Abundance ratio
NUP214	Nuclear pore complex protein Nup214	37	2.54x10 ⁷	284.92
NUP98	Nuclear pore complex protein Nup98-Nup96	19	7.28x10 ⁶	233.98
NUP50	Nuclear pore complex protein Nup50	21	1.10x10 ⁷	60.41
NUP153	Nucleoporin 153kDa, isoform CRA_a	52	3.78x10 ⁷	55.58
RANBP2	E3 SUMO-protein ligase RanBP2	64	2.85x10 ⁷	43.15
NUP88	Nuclear pore complex protein Nup88	20	1.03x10 ⁷	42.98
RAE1	mRNA export factor	10	2.61x10 ⁶	37.94
KPNA3	Importin subunit alpha-4	6	5.05x10 ⁶	26.52
RANGAP1	Ran GTPase-activating protein 1	30	3.86x10 ⁷	15.71
SUMO1	Small ubiquitin-related modifier 1	5	5.43x10 ⁶	15.36
RAN	GTP-binding nuclear protein RAN	9	1.95x10 ⁷	11.79
KPNA4	Importin subunit alpha-3	3	6.14x10 ⁵	9.50
NUP188	Nucleoporin NUP188 homolog	8	9.37x10 ⁵	6.42
KPNA2	Importin subunit alpha-1	17	1.66x10 ⁷	4.74
NUP107	Nuclear pore complex protein Nup107	13	2.72x10 ⁶	4.74
IPO7	Importin-7	20	1.33x10 ⁷	2.19
IPO5	Importin-5	6	1.78x10 ⁶	2.13
NUP93	Nuclear pore complex protein Nup93	15	2.99x10 ⁶	1.98
CSE1L	Exportin-2	14	3.60x10 ⁶	1.35
PRPF8	Pre-mRNA-processing-splicing factor 8	47	1.36x10 ⁷	1.15
HSPA5	78 kDa glucose-regulated protein	18	9.26x10 ⁶	1.11
CAND1	Cullin-associated nedd8-dissociated protein 1	11	2.91x10 ⁶	1.07
POM121C	Nuclear envelope pore membrane protein POM121C	14	5.65x10 ⁶	*
DLGAP5	Disks large-associated protein 5	18	4.24x10 ⁶	*
NUP62	Nuclear pore glycoprotein p62	10	4.00x10 ⁶	*
NUP133	Nuclear pore complex protein Nup133	13	3.47x10 ⁶	*
KPNA6	Importin subunit alpha-7	7	1.24x10 ⁶	*
NUSAP1	Nucleolar and spindle-associated protein 1	5	9.07x10 ⁵	*
RCC1	Regulator of chromosome condensation	3	5.25x10 ⁵	*
KPNA1	Importin subunit alpha	3	4.77x10 ⁵	*
NXF1	Nuclear RNA export factor 1	3	4.29x10 ⁵	*
BRCA1	Breast cancer type 1 susceptibility protein	3	4.18x10 ⁵	*

Proteins labeled with an asterisk (*) in the “Abundance ratio” column were present in the KPNB1 BioID but absent in the mNeonGreen control. Proteins are ranked by abundance ratio.

Chapter 4: Discussion

The scaffold protein anillin is required for cytokinesis and coordinates the function of many components of the cell that regulate or are part of the contractile ring. Here, we show how binding to importins, microtubules and RhoA are coordinated to regulate anillin's function for cytokinesis. We show that importins and microtubules partially compete for anillin binding, and that lack of importin-binding could make anillin regulation by microtubules more dominant in a cell. Active RhoA enhances the interaction between anillin and importins, and anillin's localization is impaired when the interface between the RBD-C2 is weakened or when importin-binding is compromised. These results support a model where RhoA and importins feedback to enhance each other's binding to anillin. We also show that Ect2's central NLS is required for cytokinesis. Then, a BioID of importin- β 1 to identify potential targets of the Ran pathway in cytokinesis identified 206 potential new proximity interactors in mitotic cells.

Several studies revealed that astral microtubules control the localization of contractile proteins to restrict them to the equatorial cortex for ring assembly. As described in the introduction, weak Nocodazole treatment in cultured mammalian cells causes an increase in the breadth of localization (Murthy and Wadsworth 2008; van Oostende Triplet et al. 2014) . In *C. elegans* several studies showed that there are separable astral vs. central spindle-directed furrows that can be induced via the displacement of centrosomes and/or reduction in microtubules via tubulin mutants (Werner et al. 2007; Tse et al. 2012). Further, a minimum density of microtubules is required to permit the formation of a ring in both *C. elegans* and fused Ptk1 cells (Canman et al. 2003; Dechant and Glotzer 2003). We found that extending astral microtubules by depleting MCAK, an enzyme that depolymerizes microtubules, narrows the breadth of anillin accumulation (van Oostende Triplet et al. 2014). And in both *C. elegans* and cultured human cells, anillin re-localizes to Taxol-stabilized microtubules (Tse et al. 2011; van Oostende Triplet et al. 2014). Recently, we found that importins also regulate anillin localization. Mutating the C-terminal NLS

to disrupt importin-binding delays anillin's cortical recruitment where it localizes to a narrow region at the equatorial cortex and cells fail cytokinesis (Beaudet et al. 2017). Thus, since both MCAK RNAi and the NLS mutant caused similar effects on anillin localization, and both microtubules and importins bind to the C2 domain and require basic residues, we determined how the NLS mutant affects microtubule-binding and if their binding is competitive and/or cooperative. We also determined how MCAK RNAi and the NLS mutant affects anillin's cortical properties. Using co-sedimentation assays, we show that importins and microtubules have the potential to bind at overlapping sites and partially compete for anillin-binding (**Figure 6**). Our FRAP experiments show that mutating the NLS and extending astral microtubules had similar maximum fluorescence recoveries indicating similar shifts of protein into the immobile fraction (73.6% and 77.2%, respectively; **Figure 7C**), while mutating the NLS increased anillin's kinetics at the membrane. These results suggest that impairing importin-binding by mutating the NLS could potentially shift anillin to be more dominantly regulated by microtubules, hence the similar immobile fractions (**Figure 7C**). However, the faster fluorescence recovery rate unique to the NLS mutant indicates that importins regulate a cortical property of anillin that is distinct from microtubules.

Previous work from our lab suggested that microtubules and the cortex/RhoA compete for anillin-binding. As mentioned above, stabilizing microtubules with Taxol causes anillin to shift from the cortex to microtubules, while decreasing active RhoA using an inhibitor (C3 transferase) or depleting Ect2 also shifts anillin to microtubules (van Oostende Triplet et al. 2014). These data show an interplay between the cortex/RhoA and microtubules. Here, our FRAP experiments indicate that perturbing importin-binding could favour microtubule-regulation of anillin, yet importins could regulate a cortical property of anillin distinct from microtubules (**Figure 8D**). Mutating the NLS and impairing importin-binding weakens anillin's cortical recruitment, possibly because it cannot stabilize the conformation required for an ideal hand-off to phospholipids, which could favour regulation of anillin by microtubules. This could explain why anillin localization shifts

to microtubules when importin-binding is impaired or when active RhoA is decreased. The faster kinetics observed with the NLS mutant may be due to decreased RhoA-anillin binding at the membrane.

When we found that importin-binding could regulate anillin's localization and function, we also uncovered autoinhibition between the RBD and C2 domains (Beaudet et al. 2017). For example, a smaller C2 fragment containing the NLS is nuclear while a larger fragment that contains both the RBD and C2 domains is not. In addition, removal of the RBD enhances both importin- and microtubule-binding to the C2 fragment in pulldown assays (Beaudet et al. 2017). These results led us to propose a model where active RhoA-binding to the RBD is required to relieve auto-inhibition of the C2 domain to make it accessible for binding to interactors. For example, microtubules, importins and phospholipids all bind to a similar region in the C2 domain and have been shown or are predicted to be inhibited by the RBD. To test this model, we changed the levels of active RhoA in cells by overexpressing or depleting the RhoGEF Ect2, and found that importin-binding was stronger when the levels of active RhoA were higher (**Figure 8B**). Using mutations to weaken the RBD-C2 interface, demonstrated that this interface is crucial for anillin's recruitment to the equatorial membrane (**Figure 8D**). Importin-binding is enhanced to this mutant, which could outcompete phospholipids and prevent the cooperative binding required with RhoA for membrane localization (**Figure 9**). Thus, anillin is auto-inhibited until anaphase when active RhoA levels increase and become sufficient to relieve this auto-inhibition. Importin-binding then stabilizes the open conformation, but does so with an affinity that permits hand-off to phospholipids for cooperative binding with RhoA to enrich anillin at the equatorial cortex (Sun et al., 2015; Beaudet et al., 2020).

Interestingly, anillin was shown to concentrate PI(4,5)P2 at the cortex, a class of phospholipids that is enriched in the equatorial membrane (Budnar et al. 2019). RhoA and anillin were previously shown to have a preference for these lipids (Frenette et al., 2012). Budnar et al.

(2019) proposed a model where anillin enhances RhoA's residence time at the membrane by locally concentrating PI(4,5)P₂ at the cleavage furrow, and thus promotes RhoA signaling to downstream effectors. This model is consistent with previous observations that anillin stabilizes RhoA at the cortex (Piekny and Glotzer 2008; Frenette et al. 2012).

So far our studies have focused on anillin as a target of the Ran pathway, but we propose that other cytokinesis proteins with NLS sequences also could be targets of this pathway. In particular, Ect2, the activator of RhoA, has a bipartite NLS in its central S-loop domain. Previous studies showed that overexpressing N-terminal fragments of Ect2 lacking the NLS have dominant-negative effects and cause multinucleation presumably due to abscission failure (Saito et al. 2003; Chalamalasetty et al. 2006). Another study showed that over-expression of full-length Ect2 with point mutations in the NLS caused transformation (a property that can be used to read out for Ect2 activity), but not when they were intact (Saito et al., 2004). These studies attribute a function to the NLS that is relevant for cytokinesis, but it is not clear what that function is. Chalamalasetty et al. (2006) proposed that the abscission defect caused by the Ect2 fragment was because it could not be nuclear localized and was retained at the midbody. The current model is that the C-terminus of Ect2 is inhibited by the N-terminal BRCT domains, which bind to a phosphopeptide motif formed by phosphorylation of T342 by Cdk1 in metaphase. In anaphase, when Cdk1 activity decreases, Ect2 is dephosphorylated, which presumably would weaken this interaction. In addition, CYK-4 is phosphorylated by Plk1, which favors binding to the BRCT domains of Ect2. Together, these induce conformational changes that make the DH/PH domains accessible for the activation of RhoA (**Figure 10B**). We propose an alternate model where importin-binding also could regulate Ect2 function by binding to the S-loop and inducing or stabilizing the open conformation (**Figure 10C**). Previous studies showed that importin-binding is inhibited by Cdk1 phosphorylation of T342, which would ensure that importins do not bind until anaphase, when Ect2 activity is required (Suzuki et al., 2015). Our results show that mutating the NLS abrogates

the ability of myc-tagged Ect2 to rescue cytokinesis failure caused by Ect2-depletion (**Figure 11B**). These preliminary results suggest that importin regulation is relevant for Ect2 function in cytokinesis. However, studying the role of the NLS in more detail will require more sophisticated experiments that include live imaging. To do this, we fused mNeonGreen to the C-terminal end of Ect2 and added a linker [(EAAAK)₃]. The localization of this construct in live cells matched the localization observed using antibodies in fixed cells (**Figure 12**; Tatsumoto et al. 1999; Yüce et al. 2005; Frenette et al. 2012). Next, we are building similar constructs using mCherry in place of mNeonGreen. Using CRISPR, we endogenously tagged Ect2 with mNeonGreen in HEK293 cells. This cell line will give us a visual readout of Ect2 depletion, while expressing mCherry-tagged Ect2 constructs in this cell line will allow us to study Ect2 mutants in live cells. We also will express other markers to characterize the phenotypes caused by mutations in the NLS.

Although we have emphasized the T342 site and its importance in regulating Ect2, recent studies showed that there is another Cdk1 site at S345 (Suzuki et al., 2015). Whereas phosphorylation of Thr342 regulates the auto-inhibition of Ect2, the role of phosphorylated Ser345 is not clear (Yüce et al. 2005; Hara et al. 2006). Given its proximity to Thr342, a role for this site in also contributing to auto-inhibition may simply have been overlooked. This same study proposed that this site is within the NLS (the consensus for Cdk1 sites are S/TPx(x)R/K) and showed that importin-binding is blocked by phosphorylation at either T342 or S345 (Suzuki et al. 2015). Although Suzuki et al. (2015) did not do any functional studies, we need to consider that phenotypes caused by our mutants could be caused by impaired phospho-regulation of T342 or S345 given their proximity to our mutant (347RKRRR351- AAAAA). Thus, we have generated a different NLS mutant (348KRR350 – AAA) with fewer mutations than our previous mutant and are performing rescue assays with this mutant. Software that predicts NLS sites consistently predicts the NLS we are studying as a bipartite classic NLS, which binds to importin-alpha/beta. However, another study showed that mutating 371RKR373 to AAA also abolishes Ect2 nuclear localization

(Liot et al. 2011). While this site is only poorly predicted and it is not clear if this is a unique NLS site, or part of the bipartite site, we could consider making mutations at this location to better separate importin-binding and phospho-regulation of Ect2.

Given the role of importin-binding in anillin regulation and our preliminary results with the Ect2 NLS mutant, we sought to identify additional cortical targets of the Ran pathway for cytokinesis. We used a proximity-labeling approach (BioID) to probe the interactome of importin- β 1 in cells synchronized for mitotic exit. We identified 238 potential proximity interactors, of which 32 had been identified by other groups (**Figure 9B**). DAVID analysis showed that our data set was enriched in cell adhesion and nuclear import proteins (**Figure 13C**). Within our data set, we identified several cytoskeletal proteins with the potential to regulate cytokinesis: DIAPH3 (or mDia2), MARCKS, SCYL1, CD2AP, ARHGAP35 (or RhoGAPp190A), and CALD1. The actin nucleator DIAPH3 is an effector of RhoA and localizes to the cleavage furrow in an anillin-dependent manner (Watanabe et al. 2010; Chen et al. 2017). Depletion of the actin-binding protein MARCKS was shown to decrease F-actin and delay mitosis, although it is unclear if MARCKS can play a direct role in cytokinesis (Rombouts et al. 2012). Similarly, depletion of the kinase SCYL1 causes cytokinesis failure (Wang et al. 2015). Other studies have shown that CD2AP, ARHGAP35 and CALD1 can interact with anillin and/or RhoA, as well as other proteins to influence the cytoskeleton in cell division (Li et al. 2003; Eppinga et al. 2006; Haglund et al. 2010; Manukyan et al. 2015). However, aside from this BioID, only DIAPH3 and MARCKS have previously been shown to interact with importins (Miki et al. 2009; Shao et al. 2015; Eustace et al. 2019). Whether these proteins are regulated by importins for cytokinesis is an exciting question.

While encouraging, we aim to repeat this experiment using Cdk1 inhibition to cause a more robust mitotic exit than in our current design (Niiya et al. 2005). Strong inhibition of Cdk1 may enrich the cell for late anaphase/early telophase complexes, which are more relevant for

cytokinesis. In addition, we will compare our data set with a list of interphase interactors (Kimura et al. 2013). Since our data was analyzed as a SILAC experiment even though BioID is a radiolabel-free method, we may analyze our data set in parallel using SAINT (significance analysis of interactome), a computational tool designed for the analysis MS data generated by radiolabel-free methods and often used for BioID data sets (Choi et al. 2011; Teo et al. 2014; Teo et al. 2016).

To our knowledge, only one other group has published a mitotic interactome of importin- β 1. Di Francesco et al. (2018) used affinity-purification/mass spectrometry to identify 272 putative interactors, followed by a validation step using a proximity ligation assay. Here, we chose BioID to isolate weak or transient importin- β 1 interactors. Proteins which bind weakly to the bait are susceptible to be lost during washing steps in other affinity purification methods. Since streptavidin binds biotin with femtomolar affinity, proteins for which interaction with importin- β 1 is weak but functionally important are presumably more likely to be recovered with BioID. Moreover, the recent design of the TurboID/miniTurbo biotin ligase variants made BioID an appealing approach since it allowed us to decrease biotinylation times to 30 minutes vs. 16 hours in conventional BioID (Branon et al. 2018). Additionally, Di Francesco et al. (2018) synchronized cells by inhibiting Cdk1 activity for 20 hours, followed by release in inhibitor-free media (Di Francesco et al. 2018). Although this has been shown to be a viable method for synchronizing cells in G2/M phase, Cdk1 activity is required for mitotic entry and its inhibition is required for mitotic exit (Vassilev et al. 2006). Thus, this approach may favour early (prometaphase and metaphase) vs. late (anaphase and telophase) mitotic protein complexes and their list would not contain proteins required for cytokinesis. We believe that combining low nocodazole treatment and Cdk1 inhibition will cause a more robust mitotic exit and enrich for anaphase-telophase complexes (Niiya et al. 2005).

The goal of our BioID experiments is to identify new targets of the Ran pathway in cytokinesis. After obtaining a list of potential targets, we need to validate these proteins for roles in cytokinesis and as targets of the Ran pathway. In addition to grouping proteins by function, we will determine if the protein has an NLS by using different NLS predictor programs (e.g. NLSdb, NLSstradamus, NLSmapper or LocSigDB). Next, we will determine if there are any relevant publications showing importin-target interactions. Depending on what is known about the function of the protein, and if studies have been done on the NLS, then we will either; 1) generate constructs for localization studies and rescue assays similar to our approach with anillin and Ect2, or 2) the list will be refined by screening potential candidates for functions in cytokinesis in *C. elegans* using dsRNA obtained from existing libraries. Since our lab also uses *C. elegans* as a model system, we have established protocols in the lab for performing RNAi, and for filming cytokinesis in the early embryo. We already have shown that the Ran pathway functions to regulate the kinetics of cytokinesis in the early embryo, and have shown that it regulates cortical contractility.

Cell division is a critical event in the cell cycle and requires extensive re-structuring of the cytoskeleton. This thesis, along with previous work from our lab, highlights a new role for Ran and importins in regulating the fundamental process of cytokinesis. Although the role of the Ran pathway as a regulator of the mitotic spindle in early mitosis is well studied, we are only beginning to understand its role in regulating proteins of the contractile ring. We show here that importins are a positive regulator of the RhoA-anillin complex, an important interaction for cytokinesis (Yüce et al. 2005; Budnar et al. 2019). Our results suggest that other contractile proteins, such as Ect2, DIAPH3 and MARCKS, among others, could be regulated by importins. Evidently, NLS(s) can act as regulatory modules in mitosis and cytokinesis. This opens new avenues of research, as the relevance of importin-binding in cytokinesis is largely unexplored. Whether binding to importins support protein complexes, as in the case of anillin and RhoA, or serve a completely different

function are exciting questions. Better understanding the role of Ran may help in the design of therapies for cancers that potentially rely on this pathway for cell division. For example, cells with higher ploidy/genomic content have a steeper Ran gradient, and therefore may depend more heavily on the Ran pathway for cytokinesis (Hasegawa et al. 2013). Going forward, elucidating the role that Ran and importins play will contribute to a deeper understanding of cytokinesis regulation.

Chapter 5: References

- Adriaans IE, Basant A, Ponsioen B, Glotzer M, Lens SMA. 2019. PLK1 plays dual roles in centralspindlin regulation during cytokinesis. *J. Cell Biol.* 218:1250–1264. doi:10.1083/jcb.201805036.
- Albee AJ, Tao W, Wiese C. 2006. Phosphorylation of maskin by Aurora-A is regulated by RanGTP and importin β . *J. Biol. Chem.* 281:38293–38301. doi:10.1074/jbc.M607203200.
- Alberts AS. 2001. Identification of a Carboxyl-terminal Diaphanous-related Formin Homology Protein Autoregulatory Domain. *J. Biol. Chem.* 276:2824–2830. doi:10.1074/jbc.M006205200.
- Basant A, Lekomtsev S, Tse YC, Zhang D, Longhini KM, Petronczki M, Glotzer M. 2015. Aurora B Kinase Promotes Cytokinesis by Inducing Centralspindlin Oligomers that Associate with the Plasma Membrane. *Dev. Cell* 33:204–215. doi:10.1016/j.devcel.2015.03.015.
- Beaudet D, Akhshi T, Phillipp J, Law C, Piekny A. 2017. Active Ran regulates anillin function during cytokinesis. *Mol. Biol. Cell* 28:3517–3531. doi:10.1091/mbc.E17-04-0253.
- Beaudet D, Pham N, Skaik N, Piekny A. 2020. Importin binding mediates the intramolecular regulation of anillin during cytokinesis. *Mol. Biol. Cell* 31:1124–1139. doi:10.1091/mbc.E20-01-0006.
- Bement WM, Benink HA, Von Dassow G. 2005. A microtubule-dependent zone of active RhoA during cleavage plane specification. *J. Cell Biol.* 170:91–101. doi:10.1083/jcb.200501131.
- Bernhofer M, Goldberg T, Wolf S, Ahmed M, Zaugg J, Boden M, Rost B. 2018. NLSdb-major update for database of nuclear localization signals and nuclear export signals. *Nucleic Acids Res.* 46:D503–D508. doi:10.1093/nar/gkx1021.

- Blower MD, Nachury M, Heald R, Weis K. 2005. A Rae1-containing ribonucleoprotein complex is required for mitotic spindle assembly. *Cell* 121:223–234. doi:10.1016/j.cell.2005.02.016.
- Branon TC, Bosch JA, Sanchez AD, Udeshi ND, Svinkina T, Carr SA, Feldman JL, Perrimon N, Ting AY. 2018. Efficient proximity labeling in living cells and organisms with TurboID. *Nat. Biotechnol.* 36:880–898. doi:10.1038/nbt.4201.
- Bringmann H, Hyman AA. 2005. A cytokinesis furrow is positioned by two consecutive signals. *Nature* 436:731–734. doi:10.1038/nature03823.
- Budnar S, Husain KB, Gomez GA, Naghibosadat M, Varma A, Verma S, Hamilton NA, Morris RG, Yap AS. 2019. Anillin Promotes Cell Contractility by Cyclic Resetting of RhoA Residence Kinetics. *Dev. Cell* 49:894-906.e12. doi:10.1016/j.devcel.2019.04.031.
- Burkard ME, Maciejowski J, Rodriguez-Bravo V, Repka M, Lowery DM, Clauser KR, Zhang C, Shokat KM, Carr SA, Yaffe MB, et al. 2009. Plk1 self-organization and priming phosphorylation of HsCYK-4 at the spindle midzone regulate the onset of division in human cells. *PLoS Biol.* 7. doi:10.1371/journal.pbio.1000111.
- Cabernard C, Prehoda KE, Doe CQ. 2010. A spindle-independent cleavage furrow positioning pathway. *Nature* 467:91–94. doi:10.1038/nature09334.
- Canman JC, Cameron LA, Maddox PS, Straight A, Tirnauer JS, Mitchison TJ, Fang G, Kapoor TM, Salmon ED. 2003. Determining the position of the cell division plane. *Nature* 424:1074–1078. doi:10.1038/nature01860.
- Canman JC, Hoffman DB, Salmon ED. 2000. The role of pre- and post-anaphase microtubules in the cytokinesis phase of the cell cycle. *Curr. Biol.* 10:611–614. doi:10.1016/S0960-9822(00)00490-5.
- Chalamalasetty RB, Hümmer S, Nigg EA, Silljé HHW. 2006. Influence of human Ect2 depletion

- and overexpression on cleavage furrow formation and abscission. *J. Cell Sci.* 119:3008–3019. doi:10.1242/jcs.03032.
- Chen A, Akhshi TK, Lavoie BD, Wilde A. 2015. Importin β 2 Mediates the Spatio-temporal Regulation of Anillin through a Noncanonical Nuclear Localization Signal. *J. Biol. Chem.* 290:13500–13509. doi:10.1074/jbc.M115.649160.
- Chen A, Arora PD, McCulloch CA, Wilde A. 2017. Cytokinesis requires localized β -actin filament production by an actin isoform specific nucleator. *Nat. Commun.* 8. doi:10.1038/s41467-017-01231-x.
- Choi H, Larsen B, Lin ZY, Breikreutz A, Mellacheruvu D, Fermin D, Qin ZS, Tyers M, Gingras AC, Nesvizhskii AI. 2011. SAINT: Probabilistic scoring of affinity purification-mass spectrometry data. *Nat. Methods* 8:70–73. doi:10.1038/nmeth.1541.
- Clarke PR, Zhang C. 2008. Spatial and temporal coordination of mitosis by Ran GTPase. *Nat. Rev. Mol. Cell Biol.* 9:464–477. doi:10.1038/nrm2410.
- Dechant R, Glotzer M. 2003. Centrosome separation and central spindle assembly act in redundant pathways that regulate microtubule density and trigger cleavage furrow formation. *Dev. Cell* 4:333–344. doi:10.1016/S1534-5807(03)00057-1.
- Dehapiot B, Carrière V, Carroll J, Halet G. 2013. Polarized Cdc42 activation promotes polar body protrusion and asymmetric division in mouse oocytes. *Dev. Biol.* 377:202–212. doi:10.1016/j.ydbio.2013.01.029.
- Dehapiot B, Halet G. 2013. Ran GTPase promotes oocyte polarization by regulating ERM (Ezrin/Radixin/Moesin) inactivation. *Cell Cycle* 12:1672–1678. doi:10.4161/cc.24901.
- Deng M, Suraneni P, Schultz RM, Li R. 2007. The Ran GTPase Mediates Chromatin Signaling to Control Cortical Polarity during Polar Body Extrusion in Mouse Oocytes. *Dev. Cell*

12:301–308. doi:10.1016/j.devcel.2006.11.008.

Douglas ME, Davies T, Joseph N, Mishima M. 2010. Aurora B and 14-3-3 Coordinately Regulate Clustering of Centralspindlin during Cytokinesis. *Curr. Biol.* 20:927–933. doi:10.1016/j.cub.2010.03.055.

Ems-McClung SC, Zheng Y, Walczak CE. 2004. Importin α/β and Ran-GTP Regulate XCTK2 Microtubule Binding through a Bipartite Nuclear Localization Signal. *Mol. Biol. Cell* 15:46–57. doi:10.1091/mbc.e03-07-0454.

Eppinga RD, Li Y, Lin JLC, Lin JJC. 2006. Tropomyosin and caldesmon regulate cytokinesis speed and membrane stability during cell division. *Arch. Biochem. Biophys.* 456:161–174. doi:10.1016/j.abb.2006.06.015.

Eustace NJ, Anderson JC, Langford CP, Trummell HQ, Hicks PH, Jarboe JS, Mobley JA, Hjelmeland AB, Hackney JR, Pedersen RT, et al. 2019. Myristoylated alanine-rich C-kinase substrate effector domain phosphorylation regulates the growth and radiation sensitization of glioblastoma. *Int. J. Oncol.* 54:2039–2053. doi:10.3892/ijo.2019.4766.

Field CM, Alberts BM. 1995. Anillin, a contractile ring protein that cycles from the nucleus to the cell cortex. *J. Cell Biol.* 131:165–178. doi:10.1083/jcb.131.1.165.

Foe VE, Von Dassow G. 2008. Stable and dynamic microtubules coordinately shape the myosin activation zone during cytokinetic furrow formation. *J. Cell Biol.* 183:457–470. doi:10.1083/jcb.200807128.

Di Francesco L, Verrico A, Asteriti IA, Rovella P, Cirigliano P, Guarguaglini G, Schininà ME, Lavia P. 2018. Visualization of human karyopherin beta-1/importin beta-1 interactions with protein partners in mitotic cells by co-immunoprecipitation and proximity ligation assays. *Sci. Rep.* 8:1–15. doi:10.1038/s41598-018-19351-9.

- Frenette P, Haines E, Loloyan M, Kinal M, Pakarian P, Piekny A. 2012. An anillin-ect2 complex stabilizes central spindle microtubules at the cortex during cytokinesis. *PLoS One* 7. doi:10.1371/journal.pone.0034888.
- Glotzer M. 2005. The Molecular Requirements for Cytokinesis. *Science* (80-.). 307:1735–1739. doi:10.1126/science.1096896.
- Haglund K, Nezis IP, Lemus D, Grabbe C, Wesche J, Liestøl K, Dikic I, Palmer R, Stenmark H. 2010. Cindr Interacts with Anillin to Control Cytokinesis in *Drosophila melanogaster*. *Curr. Biol.* 20:944–950. doi:10.1016/j.cub.2010.03.068.
- Hara T, Abe M, Inoue H, Yu LR, Veenstra TD, Kang YH, Lee KS, Miki T. 2006. Cytokinesis regulator ECT2 changes its conformation through phosphorylation at Thr-341 in G2/M phase. *Oncogene* 25:566–578. doi:10.1038/sj.onc.1209078.
- Hasegawa K, Ryu SJ, Kaláb P. 2013. Chromosomal gain promotes formation of a steep RanGTP gradient that drives mitosis in aneuploid cells. *J. Cell Biol.* 200:151–161. doi:10.1083/jcb.201206142.
- Hickson GRX, O'Farrell PH. 2008. Rho-dependent control of anillin behavior during cytokinesis. *J. Cell Biol.* 180:285–294. doi:10.1083/jcb.200709005.
- Jantsch-Plunger V, Gönczy P, Romano A, Schnabel H, Hamill D, Schnabel R, Hyman AA, Glotzer M. 2000. CYK-4: A Rho family GTPase activating protein (GAP) required for central spindle formation and cytokinesis. *J. Cell Biol.* 149:1391–1404. doi:10.1083/jcb.149.7.1391.
- Kaláb P, Pralle A, Isacoff EY, Heald R, Weis K. 2006. Analysis of a RanGTP-regulated gradient in mitotic somatic cells. *Nature* 440:697–701. doi:10.1038/nature04589.
- Kalab P, Weis K, Heald R. 2002. Visualization of a Ran-GTP gradient in interphase and mitotic

- Xenopus egg extracts. *Science* (80-.). 295:2452–2456. doi:10.1126/science.1068798.
- Kamijo K, Ohara N, Abe M, Uchimura T, Hosoya H, Lee J-S, Miki T. 2006. Dissecting the Role of Rho-mediated Signaling in Contractile Ring Formation. *Mol. Biol. Cell* 17:43–55. doi:10.1091/mbc.e05-06-0569.
- Kim H, Guo F, Brahma S, Xing Y, Burkard ME. 2014. Centralspindlin assembly and 2 phosphorylations on MgcRacGAP by Polo-like kinase 1 initiate Ect2 binding in early cytokinesis. *Cell Cycle* 13:2952–2961. doi:10.4161/15384101.2014.947201.
- Kimura K, Ito M, Amano M, Chihara K, Fukata Y, Nakafuku M, Yamamori B, Feng J, Nakano T, Okawa K, et al. 1996. Regulation of Myosin Phosphatase by Rho and Rho-Associated Kinase (Rho-Kinase). *Science* (80-.). 273:245–248. doi:10.1126/science.273.5272.245.
- Kimura M, Okumura N, Kose S, Takao T, Imamoto N. 2013. Identification of Cargo Proteins Specific for Importin- β with Importin- α Applying a Stable Isotope Labeling by Amino Acids in Cell Culture (SILAC)-based in Vitro Transport System. *J. Biol. Chem.* 288:24540–24549. doi:10.1074/jbc.M113.489286.
- Kiyomitsu T, Cheeseman IM. 2013. Cortical dynein and asymmetric membrane elongation coordinately position the spindle in anaphase. *Cell* 154:391–402. doi:10.1016/j.cell.2013.06.010.
- Kosako H, Yoshida T, Matsumura F, Ishizaki T, Narumiya S, Inagaki M. 2000. Rho-kinase/ROCK is involved in cytokinesis through the phosphorylation of myosin light chain and not ezrin/radixin/moesin proteins at the cleavage furrow. *Oncogene* 19:6059–6064. doi:10.1038/sj.onc.1203987.
- Kotadia S, Montembault E, Sullivan W, Royou A. 2012. Cell elongation is an adaptive response for clearing long chromatid arms from the cleavage plane. *J. Cell Biol.* 199:745–753.

doi:10.1083/jcb.201208041.

Kotýnková K, Su KC, West SC, Petronczki M. 2016. Plasma Membrane Association but Not Midzone Recruitment of RhoGEF ECT2 Is Essential for Cytokinesis. *Cell Rep.* 17:2672–2686. doi:10.1016/j.celrep.2016.11.029.

Lekomtsev S, Su KC, Pye VE, Blight K, Sundaramoorthy S, Takaki T, Collinson LM, Cherepanov P, Divecha N, Petronczki M. 2012. Centralspindlin links the mitotic spindle to the plasma membrane during cytokinesis. *Nature* 492:276–279. doi:10.1038/nature11773.

Lewellyn L, Dumont J, Desai A, Oegema K. 2010. Analyzing the Effects of Delaying Aster Separation on Furrow Formation during Cytokinesis in the *Caenorhabditis elegans* Embryo. Wang Y-L, editor. *Mol. Biol. Cell* 21:50–62. doi:10.1091/mbc.e09-01-0089.

Li Y, Wessels D, Wang T, Lin JLC, Soll DR, Lin JJC. 2003. Regulation of caldesmon activity by Cdc2 kinase plays an important role in maintaining membrane cortex integrity during cell division. *Cell. Mol. Life Sci.* 60:198–211. doi:10.1007/s000180300014.

Liot C, Seguin L, Siret A, Crouin C, Schmidt S, Bertoglio J. 2011. APC cdh1 mediates degradation of the oncogenic Rho-GEF Ect2 after mitosis. *PLoS One* 6. doi:10.1371/journal.pone.0023676.

Mangal S, Sacher J, Kim T, Osório DS, Motegi F, Carvalho AX, Oegema K, Zanin E. 2018. TPXL-1 activates Aurora A to clear contractile ring components from the polar cortex during cytokinesis. *J. Cell Biol.* 217:837–848. doi:10.1083/jcb.201706021.

Manukyan A, Ludwig K, Sanchez-Manchinelly S, Parsons SJ, Todd Stukenberg P. 2015. A complex of p190RhoGAP-A and anillin modulates RhoA-GTP and the cytokinetic furrow in human cells. *J. Cell Sci.* 128:50–60. doi:10.1242/jcs.151647.

Matsumura F, Ono S, Yamakita Y, Totsukawa G, Yamashiro S. 1998. Specific localization of

- serine 19 phosphorylated myosin II during cell locomotion and mitosis of cultured cells. *J. Cell Biol.* 140:119–129. doi:10.1083/jcb.140.1.119.
- McIntosh JR. 2016. Mitosis. *Cold Spring Harb. Perspect. Biol.* 8:a023218. doi:10.1101/cshperspect.a023218.
- Miki T, Okawa K, Sekimoto T, Yoneda Y, Watanabe S, Ishizaki T, Narumiya S. 2009. mDia2 shuttles between the nucleus and the cytoplasm through the importin- α/β - and CRM1-mediated nuclear transport mechanism. *J. Biol. Chem.* 284:5753–5762. doi:10.1074/jbc.M806191200.
- Mishima M, Kaitna S, Glotzer M. 2002. Central spindle assembly and cytokinesis require a kinesin-like protein/RhoGAP complex with microtubule bundling activity. *Dev. Cell* 2:41–54. doi:10.1016/S1534-5807(01)00110-1.
- Murthy K, Wadsworth P. 2008. Dual role for microtubules in regulating cortical contractility during cytokinesis. *J. Cell Sci.* 121:2350–2359. doi:10.1242/jcs.027052.
- Nair R, Carter P, Rost B. 2003. NLSdb: Database of nuclear localization signals. *Nucleic Acids Res.* 31:397–399. doi:10.1093/nar/gkg001.
- Niyya F, Xie X, Lee KS, Inoue H, Miki T. 2005. Inhibition of cyclin-dependent kinase 1 induces cytokinesis without chromosome segregation in an ECT2 and MgcRacGAP-dependent manner. *J. Biol. Chem.* 280:36502–36509. doi:10.1074/jbc.M508007200.
- Oegema K, Savoian MS, Mitchison TJ, Field CM. 2000. Functional analysis of a human homologue of the *Drosophila* actin binding protein anillin suggests a role in cytokinesis. *J. Cell Biol.* 150:539–551. doi:10.1083/jcb.150.3.539.
- van Oostende Triplet Chloe, Garcia MJ, Bik HH, Beaudet D, Piekny A, van Oostende Triplet C., Jaramillo Garcia M, Haji Bik H, Beaudet D, Piekny A. 2014. Anillin interacts with

- microtubules and is part of the astral pathway that defines cortical domains. *J. Cell Sci.* 127:3699–3710. doi:10.1242/jcs.147504.
- Oughtred R, Stark C, Breikreutz B-J, Rust J, Boucher L, Chang C, Kolas N, O'Donnell L, Leung G, McAdam R, et al. 2019. The BioGRID interaction database: 2019 update. *Nucleic Acids Res.* 47:D529–D541. doi:10.1093/nar/gky1079.
- Petronczki M, Glotzer M, Kraut N, Peters JM. 2007. Polo-like Kinase 1 Triggers the Initiation of Cytokinesis in Human Cells by Promoting Recruitment of the RhoGEF Ect2 to the Central Spindle. *Dev. Cell* 12:713–725. doi:10.1016/j.devcel.2007.03.013.
- Piekny A, Werner M, Glotzer M. 2005. Cytokinesis: Welcome to the Rho zone. *Trends Cell Biol.* 15:651–658. doi:10.1016/j.tcb.2005.10.006.
- Piekny AJ, Glotzer M. 2008. Anillin Is a Scaffold Protein That Links RhoA, Actin, and Myosin during Cytokinesis. *Curr. Biol.* 18:30–36. doi:10.1016/j.cub.2007.11.068.
- Rankin KE, Wordeman L. 2010. Long astral microtubules uncouple mitotic spindles from the cytokinetic furrow. *J. Cell Biol.* 190:35–43. doi:10.1083/jcb.201004017.
- Rodrigues NTL, Lekomtsev S, Jananji S, Kriston-Vizi J, Hickson GRX, Baum B. 2015. Kinetochores-localized PP1-Sds22 couples chromosome segregation to polar relaxation. *Nature* 524:489–492. doi:10.1038/nature14496.
- Rombouts K, Mello T, Liotta F, Galli A, Caligiuri A, Annunziato F, Pinzani M. 2012. MARCKS actin-binding capacity mediates actin filament assembly during mitosis in human hepatic stellate cells. *Am. J. Physiol. - Cell Physiol.* 303:357–367. doi:10.1152/ajpcell.00093.2012.
- Saito S, Liu XF, Kamijo K, Raziuddin R, Tatsumoto T, Okamoto I, Chen X, Lee CC, Lorenzi M V., Ohara N, et al. 2004. Deregulation and Mislocalization of the Cytokinesis Regulator ECT2 Activate the Rho Signaling Pathways Leading to Malignant Transformation. *J. Biol. Chem.*

279:7169–7179. doi:10.1074/jbc.M306725200.

Saito S, Tatsumoto T, Lorenzi M V., Chedid M, Kapoor V, Sakata H, Rubin J, Miki T. 2003. Rho Exchange Factor ECT2 Is Induced by Growth Factors and Regulates Cytokinesis Through the N-Terminal Cell Cycle Regulator-Related Domains. *J. Cell. Biochem.* 90:819–836. doi:10.1002/jcb.10688.

Schatz CA, Santarella R, Hoenger A, Karsenti E, Mattaj IW, Gruss OJ, Carazo-Salas RE. 2003. Importin α -regulated nucleation of microtubules by TPX2. *EMBO J.* 22:2060–2070. doi:10.1093/emboj/cdg195.

Shao X, Kawauchi K, Shivashankar G V., Bershadsky AD. 2015. Novel localization of formin mDia2: importin β -mediated delivery to and retention at the cytoplasmic side of the nuclear envelope. *Biol. Open* 4:1569–1575. doi:10.1242/bio.013649.

Somers WG, Saint R. 2003. A RhoGEF and Rho family GTPase-activating protein complex links the contractile ring to cortical microtubules at the onset of cytokinesis. *Dev. Cell* 4:29–39. doi:10.1016/S1534-5807(02)00402-1.

Straight AF, Field CM, Mitchison TJ. 2005. Anillin Binds Nonmuscle Myosin II and Regulates the Contractile Ring. *Mol. Biol. Cell* 16:193–201. doi:10.1091/mbc.e04-08-0758.

Su KC, Takaki T, Petronczki M. 2011. Targeting of the RhoGEF Ect2 to the Equatorial Membrane Controls Cleavage Furrow Formation during Cytokinesis. *Dev. Cell* 21:1104–1115. doi:10.1016/j.devcel.2011.11.003.

Sun L, Guan R, Lee IJ, Liu Y, Chen M, Wang J, Wu JQ, Chen Z. 2015. Mechanistic Insights into the Anchorage of the Contractile Ring by Anillin and Mid1. *Dev. Cell* 33:413–426. doi:10.1016/j.devcel.2015.03.003.

Suzuki K, Sako K, Akiyama K, Isoda M, Senoo C, Nakajo N, Sagata N. 2015. Identification of

- non-Ser/Thr-Pro consensus motifs for Cdk1 and their roles in mitotic regulation of C2H2 zinc finger proteins and Ect2. *Sci. Rep.* 5:1–9. doi:10.1038/srep07929.
- Szkarczyk D, Gable AL, Lyon D, Junge A, Wyder S, Huerta-Cepas J, Simonovic M, Doncheva NT, Morris JH, Bork P, et al. 2019. STRING v11: protein–protein association networks with increased coverage, supporting functional discovery in genome-wide experimental datasets. *Nucleic Acids Res.* 47:D607–D613. doi:10.1093/nar/gky1131.
- Tatsumoto T, Xie X, Blumenthal R, Okamoto I, Miki T. 1999. Human Ect2 Is an Exchange Factor for Rho Gtpases, Phosphorylated in G2/M Phases, and Involved in Cytokinesis. *J. Cell Biol.* 147:921–928. doi:10.1083/jcb.147.5.921.
- Teo G, Koh H, Fermin D, Lambert JP, Knight JDR, Gingras AC, Choi H. 2016. SAINTq: Scoring protein–protein interactions in affinity purification – mass spectrometry experiments with fragment or peptide intensity data. *Proteomics* 16:2238–2245. doi:10.1002/pmic.201500499.
- Teo G, Liu G, Zhang J, Nesvizhskii AI, Gingras AC, Choi H. 2014. SAINTexpress: Improvements and additional features in Significance Analysis of INTeractome software. *J. Proteomics* 100:37–43. doi:10.1016/j.jprot.2013.10.023.
- Tsai MY, Wiese C, Cao K, Martin O, Donovan P, Ruderman J, Prigent C, Zheng Y. 2003. A Ran signalling pathway mediated by the mitotic kinase Aurora A in spindle assembly. *Nat. Cell Biol.* 5:242–248. doi:10.1038/ncb936.
- Tsai MYM-Y, Wang S, Heidinger JM, Shumaker DK, Adam SA, Goldman RD, Zheng Y. 2006. A mitotic lamin B matrix induced by RanGTP required for spindle assembly. *Science* (80-.). 311:1887–1893. doi:10.1126/science.1122771.
- Tse YC, Piekny A, Glotzera M, Glotzer M. 2011. Anillin promotes astral microtubule-directed

- cortical myosin polarization. *Mol. Biol. Cell* 22:3165–3175. doi:10.1091/mbc.E11-05-0399.
- Tse YC, Werner M, Longhini KM, Labbe JC, Goldstein B, Glotzer M. 2012. RhoA activation during polarization and cytokinesis of the early *Caenorhabditis elegans* embryo is differentially dependent on NOP-1 and CYK-4. *Mol. Biol. Cell* 23:4020–4031. doi:10.1091/mbc.E12-04-0268.
- Vassilev LT, Tovar C, Chen S, Knezevic D, Zhao X, Sun H, Heimbrosk DC, Chen L. 2006. Selective small-molecule inhibitor reveals critical mitotic functions of human CDK1. *Proc. Natl. Acad. Sci.* 103:10660–10665. doi:10.1073/pnas.0600447103.
- Walczak CE, Heald R. 2008. Mechanisms of Mitotic Spindle Assembly and Function. *Int. Rev. Cytol.* 265:111–158. doi:10.1016/S0074-7696(07)65003-7.
- Wang J, Liu M, Chen L, Chan THM, Jiang L, Yuan YF, Guan XY. 2015. Overexpression of N-terminal kinase like gene promotes tumorigenicity of hepatocellular carcinoma by regulating cell cycle progression and cell motility. *Oncotarget* 6:1618–1630. doi:10.18632/oncotarget.2730.
- Watanabe S, Okawa K, Miki T, Sakamoto S, Morinaga T, Segawa K, Arakawa T, Kinoshita M, Ishizaki T, Narumiya S. 2010. Rho and Anillin-dependent Control of mDia2 Localization and Function in Cytokinesis. Chang F, editor. *Mol. Biol. Cell* 21:3193–3204. doi:10.1091/mbc.e10-04-0324.
- Weaver LN, Ems-McClung SC, Chen SHR, Yang G, Shaw SL, Walczak CE. 2015. The Ran-GTP gradient spatially regulates XCTK2 in the spindle. *Curr. Biol.* 25:1509–1514. doi:10.1016/j.cub.2015.04.015.
- Werner M, Munro E, Glotzer M. 2007. Astral Signals Spatially Bias Cortical Myosin Recruitment to Break Symmetry and Promote Cytokinesis. *Curr. Biol.* 17:1286–1297.

doi:10.1016/j.cub.2007.06.070.

Wolfe BA, Takaki T, Petronczki M, Glotzer M. 2009. Polo-like kinase 1 directs assembly of the HsCyk-4 RhoGAP/Ect2 RhoGEF complex to initiate cleavage furrow formation. *PLoS Biol.* 7. doi:10.1371/journal.pbio.1000110.

Yüce Ö, Piekny A, Glotzer M. 2005. An ECT2-centralspindlin complex regulates the localization and function of RhoA. *J. Cell Biol.* 170:571–582. doi:10.1083/jcb.200501097.

Zanin E, Desai A, Poser I, Toyoda Y, Andree C, Moebius C, Bickle M, Conradt B, Piekny A, Oegema K. 2013. A conserved RhoGAP limits M phase contractility and coordinates with microtubule asters to confine RhoA during Cytokinesis. *Dev. Cell* 26:496–510. doi:10.1016/j.devcel.2013.08.005.

Zhao WM, Fang G. 2005. Anillin is a substrate of anaphase-promoting complex/cyclosome (APC/C) that controls spatial contractility of myosin during late cytokinesis. *J. Biol. Chem.* 280:33516–33524. doi:10.1074/jbc.M504657200.

Zou Y, Shao Z, Peng J, Li F, Gong D, Wang C, Zuo X, Zhang Z, Wu J, Shi Y, et al. 2014. Crystal structure of triple-BRCT-domain of ECT2 and insights into the binding characteristics to CYK-4. *FEBS Lett.* 588:2911–2920. doi:10.1016/j.febslet.2014.07.019.